Chapter 3

Influence of Material Dispersion on Spectral Characteristics of Evanescent Wave Fiber Components

3.1 Overview

In fiber-optic communication systems, many special fibers such as rare-earth-doped fiber, Raman fiber, dispersive fiber, photosensitive fiber, dispersion compensation fiber, and so on, are developed for various applications and signal processing. However, special fibers are always expensive to make fiber-optic communication popular. Moreover, using special fibers can also give rise to difficulties in system managements and manipulations. The best solution is to employ fiber devices using standard single-mode fibers to reach the above mentioned functions, if possible. Therefore, it is important to investigate the material dispersion of the fiber devices so that variant kinds of fiber devices with new functions can be realized to improve the fiber-optic communication and sensing systems. This charter describes the influences of material dispersion on fiber components and their applications in fiber active and passive components.

3.2 High-Cutoff-Efficiency Fundamental-Mode Cutoff

In the beginning, discussions of fundamental-mode cutoff phenomenon resulting from material dispersion discrepancy between the fiber and dispersive materials are given. In fact, fused silica is a high phonon energy (~ 1100 cm^{-1}) material compared with other materials and, thus, short-pass filters are easy achieved. In this section, discussions of the influence of material dispersion in high-cutoff-efficiency fundamental-mode cutoff filters are provided.

3.2.1 Side-Polished Wideband Tunable Short-Pass Filters

In the literatures, a variety of materials were used as the overlay on side-polished fiber (SPF) for filters, polarizers, amplifiers, modulators and so forth [1-7]. Dispersive materials whose refractive index varies with wavelength are attractive to make tunable fiber filters and mode-field converters based on SPFs, but have not yet been reported. Tunable fiber filters are important to photonic networks in bandwidth provisioning and management. They can be achieved using dispersive fibers [8-10] based on the discrepancy of material dispersion between the core and cladding. Generally, the refractive index difference Δn of the single-mode fibers is almost wavelength-independent over the whole communication bands and each lowest order LP_{01} mode of the wavelengths is thus well-confined in core without cutoff. In contrast, Δn of a dispersive fiber, whose core and cladding have different dispersive characteristics, is wavelength-dependent and therefore the refractive index dispersion (RID) curves, $n(\lambda)$, of the core and cladding intersect at a LP_{01} mode cutoff wavelength (LP_{01}-λ_c) which divides the wavelengths into bound and refracting leaky modes. The LP_{01}-λ_c and the mode field diameter (MFD) can be adjusted through bending and local heating [11], respectively. However, the fabrication, insertion loss, crosstalk and cost of the filters using dispersive fibers show great difficulties for practical use [8-10].

Here, a wideband tunable fiber short-pass filter with the tuning range of around 400 nm (1250 ~1650 nm) based on dispersive evanescent tunneling from a side-polished single-mode fiber and a dispersive optical polymer overlay structure, shown in Fig. 3.1(a), has been reported for the first time to our knowledge. The SPF is to remove a portion of cladding away to access the evanescent field of the fiber. If the refractive index of the external overlay n_o is smaller than the mode index n_{eff} ($\equiv \beta_0/\kappa_0$, β_0 is the propagation constant at wavelength λ and $\kappa_0=2\pi/\lambda$) of the SPF, the total internal reflection (TIR) is satisfied and the wavelengths are bounded to propagate in core with the field decays monotonically in the radial direction and have no optical losses. The n_{eff} and MFD of the bound modes can be perturbed via adjusting n_o. A smaller n_o

makes the guiding light more tightly confined in core and the MFD is reduced. Oppositely, the MFD is expanded when n_o approaches the n_{eff}. On the other hand, when $n_o \geq n_{eff}$, the TIR is frustrated and the oscillatory field of the wavelengths tunnels the lower index cladding into the unbounded higher index external overlay and gives rise to significant losses. Since the n_o and n_{eff} have different wavelength dependent behaviors originated from the dispersion discrepancy between the overlay and SPF, the ratio of the evanescent tunneling is dispersive and the induced leakage losses are different for wavelengths. Accordingly, a fiber wavelength filter or a mode field converter can be obtained. For an adequate dispersive overlay, optical polymer is more flexible and usually has quite different dispersive characteristic than inorganic fiber constituents to fabricate tunable fiber short/long/band-pass filters. Its refractive index varies with temperature and therefore the corresponding LP_{01}-λ_c of the SPF moves upward or downward. The difference of the RID slopes $|dn/d\lambda|$ between the polymer overlay and the SPF is decisive to the temperature tuning ramp of the filter. A short-pass and a long-pass filter, which uses highly dispersive polymer [12] (e.g., conjugated polymer) overlay on a SPF, can be cascaded to realize a wideband tunable band-pass filter. These wideband tunable filters are useful for the tri-Band (1310/1490/1550-nm) WDM-PON system in FTTH applications and are promising as a high-resolution refractometer for liquids. In multi-mode fibers, the propagation constants and the n_{eff} are different for each guiding mode and the dispersive evanescent tunneling can be employed to make a modal filter for dispersive multiplexing [13].

In Fig. 3.1(b), the dashed gray curves are the Cauchy dispersion fit for Cargille index-matching liquids and the dashed black curve is the nominal Cauchy dispersion fit of the dispersive optical polymer OCK-433 (Nye Lubricants). For the single-mode SMF-28 (Corning) fiber, the Ge concentration of the core is approximately around 4.1 mol.% and the cladding is pure silica. The solid black and gray curves are the Sellmeier dispersion curves of the 4.1 mol.% Ge-doped core and the fused silica, respectively. The Sellmeier dispersion equations of the form:

$$n^2(\omega) = 1 + \sum_j \frac{\omega_{pj}^2}{\omega_{0j}^2 - \omega^2}$$

These equations provide data on the refractive index of materials vs. wavelength, without the need for extensive tables. They are usually valid only in high transparency spectral regions, far from resonances, where susceptibility is real. Usually, Sellmeier dispersion equation for a material may contain a pole (i.e. a resonance) at low frequency ($\omega_0 << \omega$) and one at very high frequency ($\omega_0 >> \omega$). In practice, the Sellmeier dispersion equation is expressed in terms of wavelength.

$$n^2(\omega) = 1 + A + \sum_j \frac{\lambda_{pj}^{-2}}{\lambda_{0j}^{-2} - \lambda^{-2}} - d\lambda^2$$

$$= a + \sum_j \frac{b_j \lambda^2}{\lambda^2 - c_j} - d\lambda^2$$

For silica, a good fit can be obtained and valid from 0.21 ~ 3.71 μm wavelength by using a 3-pole Sellmeier dispersion equation with poles at approximately 9.9 μm, 116 nm and 68 nm. The contributions of the individual poles can be seen as follows:

$$n(\lambda) = \sqrt{1 + A_1(\lambda) + A_2(\lambda) + A_3(\lambda)}$$

$$A_1(\lambda) = \frac{0.6961663\lambda^2}{\lambda^2 - 0.0684043^2}$$

$$A_2(\lambda) = \frac{0.4079426\lambda^2}{\lambda^2 - 0.1162414^2}$$

$$A_3(\lambda) = \frac{0.8774794\lambda^2}{\lambda^2 - 9.896161^2}$$

In Fig. 3.1(b), the Sellmeier curve intersects the certain Cauchy curve at a LP_{01}-λ_c which separates the wavelengths into bound and tunneling leaky modes. The tunneling leaky modes differ from the afore-mentioned refracting leaky modes. In our

experiments, the Cargille index liquids were used to characterize the short-pass filter resorting to their similar dispersion characteristics shown in Fig. 3.1(b). These liquids have a higher and lower dispersion (n_F-n_C) than the fused silica at visible and infrared wavelengths, respectively. We characterized two kinds of SPFs using SMF-28 and GF4A (Nufern) fiber and the fiber parameters are listed in table 3.1. The SMF-28 has a Ge-doped core and a pure silica cladding while the GF4A has a highly B/Ge co-doped core and a more highly B-doped inner cladding. Though the exact Sellmeier coefficients of the both fibers are not available, the borosilicate glass (GF4A) was found to manifest a steeper RID slope than other fiber constituents at infrared wavelengths [8].

In fabrication, a portion of the fiber jacket was stripped off and the section was then embedded and glued into the curved V-groove with radius of curvature *R* of 15 m on a silicon substrate. The silicon V-grooves were precisely etched to the desired dimension such that the central cladding thickness after polishing is around 2.7 μm and the exposed cladding was polished away using fine slurry with grain size of around 100 nm to avoid the scattering losses from scratches. In polishing, the silicon substrate surface served as an inherent stop-point due to the superior hardness than silica cladding. This saves much time for polishing. Finally, the characteristics of the well-polished fibers were calibrated by liquid-drop experiments [14]. The effective interaction length L_{eff} of the SPF is approximately proportional to $\sqrt{R}$ of the SPF and a large *R* is essential for a long L_{eff} [14]. A long L_{eff} is advantageous to attain a high power extinction ratio for the shallow-polished fiber because a deep-polished fiber (remained cladding < 0.5 μm) is substantially polarization-sensitive and is not preferred. Through the liquid-drop experiments and L-Z power attenuation formula [15], the L_{eff} was estimated to be 11 mm and 7.6 mm at 1550 nm wavelength for side-polished SMF-28 (SP-SMF-28) and GF4A (SP-GF4A), respectively. They are much longer than that of using the quartz polishing substrates [16]. By using a 1550 nm DFB laser and a polarization controller, the insertion and polarization dependent losses of the both SPFs were measured below 0.26 dB and 0.09 dB, respectively. A white-light laser, which is composed of multiple superluminescent laser diodes (SLDs) spanning 1250 ~ 1675 nm, was then launched into the SPF on which the index liquids

overlay was applied and the spacers with 250 μm diameter d were used to maintain a constant film thickness. The film is thick enough to avoid the resonance reflections from superstrate when $n_o \geq n_{eff}$ [1,7]. An optical spectrum analyzer (OSA) was used to record the spectral responses of the SPFs for different index liquid overlays.

In Fig. 3.2, the dashed lines express the initial output power spectra of the SPFs without an index liquid overlay. In Fig. 3.2(a), the initial power was attenuated due to significant Fresnel reflection loss between SMF-28 and GF4A. The spectral responses for variant Cargille index liquids (n_D value) were normalized and plotted with black lines. As the index increases, the corresponding LP_{01}-λ_c shifts toward shorter wavelength and the wavelength separation between the adjacent falling curves (index interval = 0.002) is around 90 nm and 200 nm for SP-GF4A and SP-SMF-28, respectively. For the latter, it could be advantageous to achieve a refractometer with the index sensitivity of up to 1×10^{-5} for liquids under 1 nm optical resolution. The slope of the falling curves in Fig. 3.2(a) is slightly steeper than that in Fig. 3.2(b) since the RID slope of the GF4A is higher than that of the SMF-28.

To investigate the wavelength tunability of the filter, the OCK-433 whose thermo-optic coefficient dn_D/dT, given by the supplier, is -3.6×10^{-4}/°C was applied against the fiber's polished surface and then thermally cured. OCK-433 (nominal n_D = 1.460) is an optical polysiloxane polymer and is designed for index-matching. The dn_D/dT varies almost linear from 0°C to 100°C and the index decreases with increasing temperature. The decomposition temperature is above 250°C. The cured OCK-433 was heated up to 54°C first and makes all wavelengths transmitted to OSA. The controlled temperature can be stable to 0.1°C by using a dual TE-cooler module. Subsequently, the temperature was decreased every other 3°C and the spectral responses changed accordingly shown in Fig. 3.3. All transmission power was extinguished to approach the noise level at around 39°C and the typical rejection efficiency was higher than 50 dB. From Fig. 3.3, the SP-SMF-28 is shown to function as a tunable fiber short-pass filter with the tuning range of around 400 nm (1250 ~ 1650 nm) by the temperature variations from 39°C to 54°C. Nevertheless, the experimental results were not self-consistent for the temperature was operated by

heating-up and cooling-down. For heating-up, the results can always be close to Fig. 3.3 when the controlled temperature was swiftly jumped to 54°C for a few seconds at beginning of each tuning and then dropped to a desired temperature immediately. The response times for temperature rising and falling were different for the same optical bandwidth. By raising the temperature from 45°C to 48°C, the steady time was 5.1 seconds and the corresponding optical bandwidth (wavelength separation between the wavelengths at 90% power transmission of their individual falling curves) was measured to be 141.2 nm. Accordingly, the response time for temperature rising was 36.1 ms/nm (tuning speed = 0.028 nm/ms). For the same optical bandwidth, the response time was 40.7 ms/nm (tuning speed = 0.025 nm/ms) for the temperature falling from 48°C to 45°C.

In conclusion, we have demonstrated a wideband tunable fiber short-pass filter based on a SPF with dispersive optical polymer overlay. The tuning range can be as wide as 400 nm under temperature variation of 15°C. The insertion loss is negligible and the rejection efficiency is higher than 50 dB. This readily applicable tunable component is simple and cost-effective. In principle, it can also be exploited as an accurate refractometer for liquids with the best index sensitivity of up to 1×10^{-5}.

3.2.2 Fused-Tapered Wideband Tunable Short-Pass Filter

Tunable short-pass fiber filters are advantageous for the S-band EDFAs [17] and for the high isolation WDM (de)multiplexers in triple-play (1310/1490/1550-nm) fiber-optic systems. A tunable short-pass fiber filter can be achieved by utilizing the fundamental-mode cutoff mechanism in which the lights with the wavelength longer than the cutoff wavelength λ_c can be highly attenuated to obtain efficient filtering with sharp filter skirt. The achieved cutoff efficiency is dependent on the material dispersion of the surrounding dispersive material and the waveguide dispersion of the tapered fiber device. A tunable λ_c with high cutoff efficiency is possible when the cross angle between the refractive index dispersion (RID) curves of the tapered fiber and the surrounding dispersive material is large [18]. A larger cross angle can give rise

to a steeper cutoff with higher rejection efficiency for the wavelengths longer than the cutoff wavelength. Since the absorption phonon energy of the used dispersive material (Cargille index matching liquids) is so different from the high absorption phonon energy (~ 1100 cm^{-1}) of the silica fiber glass, the spectral response will be short-pass and the cutoff wavelength can be moved upward or downward, depending on the thermo-optic coefficients (dn/dT) of the dispersive material and the applied heating temperature [18]. The dn/dT of the index liquid is -3.74×10^{-4}/°C, which is high enough to give rise to high efficient temperature-tuning. The cutoff efficiency is also influenced by the interaction length, the shape of the fused-tapered region [19] and the bending curvature of the tapered fiber. During fabrication, the flame must be traveling back-and-forth to guarantee a uniform waist with long interaction length, which can induce more attenuation for cutoff lights. This is because the long interaction length of the tapered transition will not only raise the RID curve of the tapered fiber [19] but also make the dispersion slope steeper to produce a sharper cutoff. On the other hand, the bending curvature of the tapered fiber can also change the dispersion slopes of the RID curves, since the electromagnetic field distribution will be deformed and shifted toward the outside of the bend. In this work, we investigate to achieve better cutoff efficiency by properly choosing the material and waveguide dispersions. So far our best fabricated short-pass tapered filters have the rejection efficiency of 55 dB at 1530 nm and the 55 dB isolation bandwidth is 80 nm (1450 ~ 1530 nm).

The tunable short-pass fiber filter illustrated in Fig. 3.4 is fabricated by the flame-brushing technique using a hydrogen gas to provide a wideband tunable loss window. The moving flame is properly scanned to make a uniform waist of the tapered region with a long interaction length. A single-mode fiber (SMF-28: Corning) with a section of the fiber jacket removed is heated and stretched until the desired diameter is reached. The final diameter and length of the uniform waist is respectively measured to be around 26 μm and 18 mm. The total tapered length is about 30 mm. Finally, the dispersive optical material (Cargille index-matching liquid with the index $n_D = 1.456$ and dn_D/dT of around -3.74×10^{-4}/°C) is applied to surround the tapered region of the fiber. A broadband white light source containing superluminescent diodes spanning from 1250 to 1650 nm is launched into the measured fiber for performing

measurement. The tapered fiber is heated by a TE-cooler to stabilize the temperature within 0.1°C. The refractive index of the surrounding index liquid decreases with the increasing temperature and in this way the temperature tuning from 24°C to 33°C can make the whole wavelength band from 1250 to 1650 nm become all-rejection or all-pass.

Fig. 3.5 shows the spectral responses of a fabricated short-pass filter at different temperatures. The tuning range and the tuning efficiency can be as wide as 400 nm (1250 ~ 1650 nm) and 44.4 nm/°C. The rejection efficiency at 1530 nm is 55 dB and the 55 dB isolation bandwidth is about 80 nm (1450 ~ 1530 nm). The cutoff efficiency can be judged by the dispersion slope of the filter skirt, which is measured to be 0.67 dB/nm. To investigate the influences of the strain and bending on the cutoff efficiency, another tapered fiber filter with the 30 mm tapered length and the 34-μm waist diameter is fabricated and measured. In Fig. 3.6, the dispersion slopes of the filter skirt in the tensile strain and bending conditions are different at 25°C. Two clampers are used at bilateral sides of the tapered region to control the tensile strain and bending curvature. The displacement d of the two clampers is in a positive for moving outward while is in a negative sign for moving inward conditions. For moving outward, the dispersion slope of the cutoff efficiency is almost the same whereas the cutoff wavelength moving toward shorter wavelengths. This is because the tensile strain can make the density of the tapered silica fiber decrease and thus the cross point of the RID curves of tapered fiber and the Cargille index liquid move to shorter wavelengths. On the other hand, the cutoff efficiency is gradually degraded and the cutoff wavelength moves toward shorter wavelengths when moving inward. This is because the bent tapered fiber can make the evanescent waves much easier to leak out and the evanescent coupling become less dispersive, accordingly [20]. Obviously, the straight tapered fiber filter has a higher cutoff efficiency than the bent tapered fiber under the same tapered diameter and interaction length. In this way the dispersion slope of the RID curve becomes flatter and the cutoff efficiency is degraded for the bent fiber. The fundamental-mode cutoff wavelength is also moved accordingly.

The tunability of the dispersion slope can be useful for different kinds of applications like fiber sensors and gain equalizers of optical amplifiers. The cutoff

efficiency is also highly related to the material dispersion discrepancy between the applied dispersive material and the tapered fiber. Larger difference of the absorption phonon energies between the silica fiber and the dispersive materials can result in higher cutoff efficiency and the related experimental results can be found in our previous work [18].

We have demonstrated wideband tunable (1250 ~ 1650 nm) fused-tapered short-pass fiber filters with high cutoff and temperature-tuning efficiency (44.4 nm/°C) by properly choosing the applied dispersive material and the tapered fiber structure. For silica fibers, the use of the dispersive material with lower absorption phonon energy and the tapered fiber structure with longer interaction length in a tightly straight package are the key factors to obtain a sharp fundamental-mode cutoff. The achieved rejection efficiency for the cutoff band is above 55 dB and the dispersion slope of the filter skirt is 0.67 dB/nm.

3.3 Local Fundamental-Mode Cutoff in Er^{3+}-doped Fiber

Previously, we have demonstrated high-cutoff efficiency side-polished/fused-tapered short-pass filters with tuning range of over 400 nm and rejection efficiency of above 55 dB. Based on the material dispersion relationship between dispersive material and fiber, tunable short/long/band-pass or band-rejection filters can be achieved accordingly. These filters can be further employed to make tunable fiber amplifiers and lasers by suppressing unwanted gain bandwidth of the active medium. The short-pass filters are used to achieve high-tuning efficiency fiber lasers in this section.

3.3.1 Thermo-Optic Tunable Fiber Ring Laser

Tunable fiber lasers are essential for the fiber-optic communications and sensing. The wavelength tuning range mainly depends on the gain bandwidth of the active medium and the tuning range of the filter. Both of the Raman and Er^{3+}-doped fiber amplifiers (EDFAs) can provide a very wide gain bandwidth of up to 100 nm and, for EDFAs,

the laser amplification can occur at S- (1480 ~ 1520 nm) or C- (1530 ~ 1565 nm) or L- (1570 ~ 1610 nm) bands contingent upon the erbium ion concentration, length of the erbium-doped fiber (EDF) and/or amplified spontaneous emission (ASE) suppressing filter. Tunable Er^{3+}-doped fiber lasers had been demonstrated using variant kinds of tunable filters [21-29]. Among them, the fundamental-mode cutoff wavelength (LP_{01}-λ_c) induced from a depressed inner cladding is distinguished for wideband distributed ASE suppression and was employed to achieve tunable S-band EDFAs and fiber lasers [29,30]. The depressed inner cladding in EDF modifies the waveguide dispersion, which varies the refractive index dispersion (RID) $n(\lambda)$ curves, and the effective indices of the long and short wavelengths become lower and higher than the index of the outer silica cladding, respectively [31]. The ASE peak wavelength and the longer wavelengths are substantially suppressed while the short wavelengths in S-band can thus obtain higher population inversions and sufficient amplification. The cutoff wavelength can be tuned by bending the fiber and the total distributed loss for wavelengths longer than the cutoff is > 200 dB through entire 15-m-long EDF [30]. However, the LP_{01}-λ_c induced from waveguide dispersion is only mechanically tunable and the distributed loss can only be generated at long-wavelength side of the cutoff, which is difficult to achieve tunable L-band EDFAs.

In this work, we demonstrate a high-efficiency and continuously tunable Er^{3+}-doped fiber ring laser (EDFRL) with 26 nm tuning range and 40 dB signal-ASE-ratio based on a local LP_{01}-λ_c induced from material dispersion in the ring resonator shown in Fig. 3.7(a). The LP_{01}-λ_c is thermo-optically tunable and is obtained by overlaying the side-polished fiber (SPF) with dispersive optical polymer [18] shown in Fig. 3.7(b). When the dispersion slopes $|dn/d\lambda|$ of the optical polymer and SPF are different, the $n(\lambda)$ curves can intersect at a LP_{01}-λ_c point which separates the wavelengths into bound and tunneling leaky modes to act as a wavelength filter. While the $|dn/d\lambda|$ of the SPF is steeper than that of the optical polymer, the filter will function as a short-pass filter [18]. On the contrary, the filter operates as a long-pass filter. A band-rejection or a band-pass filter [10] can also be obtained based on such kind of material dispersion discrepancy. The refractive index of the optical polymer changes with temperature and the LP_{01}-λ_c wavelength moves accordingly. The cross angle between the $n(\lambda)$ curves is

crucial to the sharpness of the cutoff, which is related to the linewidth of the fiber laser, and the thermo-optic coefficient dn_D/dT is decisive to the temperature tuning ramp. Although SPFs had been used as filters in EDFRL [25-28], this is the first time that a side-polished short-pass filter, which provides a wideband tunable (> 400 nm) loss window with high rejection efficiency (> 45 dB/cm) for wavelengths longer than the cutoff and high tuning efficiency (26.7 nm/°C), is used to investigate the EDFRL with lasing wavelength tuning toward the shorter wavelengths through an efficient local ASE suppression in the resonator. It reflects that, based on such material dispersion discrepancy, tunable fiber short/long-pass or band-rejection filters could be employed to achieve tunable EDFAs and lasers covering the S-, C-, and/or L-bands using variant optical polymers in the future.

For a high efficient local ASE suppression in EDFRL, a sharp filter edge and deep stopband are required for the tunable LP_{01}-λ_c induced from material dispersion. Fig. 3.8 shows the RID curves of the silica cladding, 4.1 mol.% Ge-doped core, the effective mode index n_i of the guiding wavelengths, Cargille index-matching liquids, and the thermo-optic polymer OCK-433 (Nye Lubricants). The 4.1 mol.% Ge-doping concentrations approximate to the core of the SMF-28 (Corning) fiber. The refractive index difference Δn between the core and cladding is almost wavelength-independent and operating wavelengths are well-confined to propagate in core without LP_{01}-λ_c. The mode field diameter (MFD) expands when the wavelength increases and the refractive index goes down simultaneously. Accordingly, the $|dn/d\lambda|$ of the n_i is steeper than that of the core and cladding. While the dispersive optical materials are applied on the SPF, the evanescent wave tunneling becomes dispersive and the RID curves intersect with each other to generate LP_{01}-λ_c ascribing to material dispersion discrepancy [18]. When the cross angle between them is larger, the LP_{01}-λ_c becomes sharper and the resulting filter edge is steeper. The $|dn/d\lambda|$ in Fig. 3.8 are n_i > Ge-doped core > cladding > OCK-433 > Cargille liquids. Thus, the LP_{01}-λ_c is short-pass filter and the corresponding cross angle will be larger by using Cargille liquids. A sharp LP_{01}-λ_c not only achieves steeper filter edge, but also contributes to higher rejection efficiency for

the stopband, which are the key factors to an efficient local ASE suppression in EDFRL.

3.3.2 Experimental Results and Discussion

In fabrication, the fiber short-pass filter is made from a SPF using SMF-28 fiber with dispersive polymer overlay [18]. A section jacket of the SMF-28 was removed and the naked fiber was then embedded in the silicon V-groove whose radius of curvature is 15 m. The exposed cladding was polished away with the polishing slurry of grain size of around 100 nm until the strong evanescent wave can be accessible. The insertion loss, polarization dependent loss, effective index n_{eff}, and effective interaction length L_{eff} of the SPF at 1550 nm wavelength were then measured to be 0.26 dB, 0.09 dB, 1.449 and 11 mm through liquid-drop test and L-Z formula fitting [18]. The Cargille liquids and OCK-433 are isotropic with no birefringence and were respectively applied on SPF with the thickness of around 1 mm while a TE-cooler (TEC) plate was placed on them with 0.1°C temperature resolution. The thermo-optic coefficient of OCK-433 is -3.6×10^{-4}/°C and thus the refractive index decreases with increasing temperature. A broadband light source (1250 ~ 1675 nm) containing multiple SuperLuminescent Diodes (SLDs) was launched into the SPF and the wavelength responses v.s. temperature variation were shown in ref. [18]. For the wavelengths longer than the LP_{01}-λ_c, they suffered strong optical losses since the refractive index n_o of the dispersive material is higher than n_{eff} of the SPF. The rejection efficiency of the short-pass filter was above 50 dB for 11-mm-long L_{eff} (> 45 dB/cm) and the tuning range was of around 400 nm (1250 ~ 1650 nm) wavelength by temperature variation of 15°C (26.7 nm/°C) [18]. By incorporating the thermo-optically tunable short-pass filter into the resonant cavity to provide a wideband tunable loss window shown in Fig. 3.7 the EDFRL was fulfilled. The EDL001 (POFC) with the length of 20 meters is our available EDF and is designed for L-band amplification. The absorption coefficients are of around 12 dB/m and 30 dB/m for 1480 nm and 1530 nm wavelength, respectively. It was pumped by a 1480 nm diode laser with a 220 mW launched power and absorbed the generated wavelengths in C-band to give amplification in the L-band.

The optical feedback was achieved by the 10% power splitting from a broadband tap coupler and the traveling-wave cavity made the ASE peak wavelength lasing. When the LP_{01}-λ_c was tuned, the unwanted ASE was suppressed and the lasing wavelength moved, accordingly. The in-line isolator restricted the EDFRL to occur in only co-propagation direction of pump light with the isolation ratio of 35 dB from 1450 nm to 1650 nm wavelength.

To investigate the influences of the sharpness of the LP_{01}-λ_c, the Cargille liquids were applied on SPF first and the pump laser was biased at current of 605 mA (optical power=140 mW). The spectral responses of the EDFRL are shown in Fig. 3.9 and the initial lasing wavelength without liquids is 1599.4 nm under 0.2 nm optical resolution of the optical spectrum analyzer. When the refractive indices 1.456 (n_D) and 1.458 (n_D) were used, the lasing wavelength moved to shorter wavelengths and the laser peak power decreased following the gain profile. The pump laser was re-biased at currents of 758 mA (175 mW) and 943 mA (205 mW) for curves 1.456 and 1.458, respectively, to attain gain saturation. Subsequently, the Cargille liquids were replaced by OCK-433 and the spectral responses are shown in Fig. 3.10 while the pump laser was biased and fixed at current of 1 A (220 mW) through the experiments. Before forming a ring cavity, the ASE peak wavelength for the 20 meters of EDL001 was measured to be 1596.6 nm. For EDFRL, the lasing wavelength when the OCK-433 was heated to 43°C to make all wavelengths passed was 1595.8 nm. The lasing wavelength (1595.8 nm) is not consistent to the initial lasing wavelength (1599.4 nm) of using the Cargille liquids due to the fusion splicing between the SMF-28 and EDL001. Their fiber structures are so different and thus the conditions of each splicing were not identical, which made the initial lasing wavelengths different. When the temperature of the TEC was cooling down, the lasing wavelengths were again moving toward shorter wavelengths and the peak power was gradually reduced following the gain profile of the EDF. While the temperature was tuned to 39.6°C, the lasing wavelength was 1569.8 nm and was at the short wavelength edge of the ASE. Thus, the tuning range of the EDFRL is 26 nm by temperature variation by 3.4°C and the typical signal-ASE-ratio is above 40 dB.

From Fig. 3.10, the ASE becomes conspicuous at 39.6°C since the ASE peak was at 1596.6 nm and thus the residual ASE were accumulated and propagated in fiber. The residual ASE can be eliminated if the short-pass filter was placed just right before the laser output. At 39.6°C, the inset plot in Fig. 3.10 shows the laser spectrum near the edge of the gain bandwidth and where the comb-like filtering phenomenon reflects the resonant coupling between the SPF and the top surface of the optical polymer, which occurs only when n_o is substantially higher than the n_{eff} [27]. The resonance spacing is around 0.79 nm and the resonant coupling can be eliminated by inducing roughness on top surface of the polymer or enhanced by improving the finesse to serve as a DWDM filter based on our SPFs with a very long L_{eff}. In Fig. 3.9 and 3.10, the laser linewidth broadens and the wavelength-tuning efficiency increases when lasing wavelength moves downward and the measurements of laser linewidth are listed in table 3.2. The mean FWHM linewidth is around 0.5 nm, which means that the EDFRL is not under the single-longitudinal-mode operation because the tap coupler can not play as a high Q resonator, and the laser linewidth is related to the cross angle between RID curves. When the lasing wavelength moves downward, the laser linewidth broadens since the emission cross-sections of the erbium ions gradually decreases at short wavelengths, (see ASE spectrum in Fig. 3.10). Although the gain profile inclines to gradually decrease at the left-half part of the ASE, which is advantageous for the guided peak wavelength to strongly lase, the spectral curves, falling toward lower-right, of the short-pass filter will compensate the inclination [18]. Therefore, the amplification for the guided peak wavelength is not as strong as before and the optical gain is robbed by adjacent wavelengths to induce linewidth broadening. As to the tuning efficiency, it was enhanced by similar reasons when lasing wavelength moved downward and is related to the sharpness of the cutoff. Actually, the guided peak wavelength is determined by the superposition of the overall emission cross-sections from the whole EDF and the suppression spectra of the local short-pass filter. For an ideal short-pass filter with an abruptly sharp LP_{01}-λ_c, the lasing wavelength will occur at the edge and moves with the tuning. However, the cutoff can not be very sharp for real short-pass filters and thus the lasing wavelength can occur at the long-wavelength side of the cutoff for high emission cross-section area. When the LP_{01}-λ_c moves downward to the

lower emission cross-section area, the lasing wavelength can only occur at the edge of the cutoff. Tuning from high to low emission cross section area, the lasing wavelength moves faster than the LP_{01}-λ_c and thus the tuning efficiency grows up with decreasing temperature. The laser linewidth will be narrower by using the short-pass filter with sharp cutoff since the modes competitions will be highly reduced at wavelengths longer than the cutoff. From table 3.2, the 30 dB linewidth is narrower by using the Cargille liquids than the OCK-433 because the former achieves a steeper cutoff than the latter (see Fig. 3.8).

We have demonstrated a simple, high-efficiency and continuously tunable EDFRL based on an efficient local LP_{01}-λ_c using a novel wideband tunable fiber short-pass filter in ring resonator. The laser can be tuned close to the short-wavelength edge of the gain bandwidth and the tuning range is 26 nm by 3.4°C with the signal-ASE-ratio of around 40 dB. The FWHM linewidth is about 0.5 nm and is related to the cross angle between RID curves. The short-pass filter provides widely thermo-optically tunable local ASE suppression with high rejection efficiency (> 45 dB/cm) for the wavelengths longer than the cutoff. Based on our investigation, a novel fiber with distributed LP_{01}-λ_c for tunable EDFAs covering the S-, C-, and/or L-bands and tunable Raman amplifiers are promising and are now in progress. The single-longitudinal-mode operation for fiber lasers can be performed by exploiting a wideband high Q resonator, e.g. dielectric coating, in future works.

3.4 Discrete Fundamental-Mode Cutoff in Er^{3+}-Doped Fiber

A short-pass filter can be used to obtain a tunable fiber laser by suppressing the longer wavelengths. However, a short-pass filter is inefficient to achieve tunable fiber amplifier. This dissertation demonstrates tunable fiber amplifier by using multistage short-pass filters, which can efficiently suppress longer wavelengths to squeeze gain for shorter wavelengths, in Er^{3+}-doped fiber here.

3.4.1 S- and C + L-Bands EDFA

S-band (1480 ~ 1520 nm) has been recently studied as a new frequency band for fiber-optic communication and where the thulium-doped fluoride fiber [32], Raman fiber [33], erbium-doped fiber (EDF) [29,30], and other methods [34-37] were proposed to obtain optical gain in the S-band. Among them, the thulium and Raman are both complicated in using special fibers which are not compatible to the current erbium-doped fiber amplifier (EDFA) systems in the C-band (1530 ~ 1565 nm) and the L-band (1570 ~ 1610 nm). On the other hand, the conventional EDF does not provide gain in S-band though its emission cross section covers the S-, C-, and L-bands simultaneously. In fact, the available gain bandwidth is contingent on the Er^{3+} concentration, the upper-state population, length of the EDFs, and the amplified spontaneous emission (ASE) suppressing filters. So far, the most promising S-band EDFAs employ the EDFs with depressed inner cladding to achieve fundamental-mode cutoff λ_c at the longer wavelengths [29,30]. The depressed inner cladding in EDFs modifies the waveguide dispersion, which in terms varies the refractive index dispersion (RID) n(λ) curves. The effective indices of the longer (shorter) wavelengths become lower (higher) than the index of the outer silica cladding, respectively [31]. The ASE at the longer wavelengths can then be substantially suppressed so that in the shorter wavelengths (S-band) higher population inversion and sufficient amplification can be obtained. λ_c can be tuned toward shorter wavelengths by bending the fiber and the total distributed loss for wavelengths longer than the λ_c can be > 200 dB through an entire 15-m-long EDF. However, a specially designed EDF is required for S-band amplification [29,30]. Moreover, when the radius of bending curvature gradually decreases, the cutoff efficiency and insertion loss become worse and higher, respectively.

In contrast to the λ_c induced by waveguide dispersion, we have demonstrated widely tunable (1250 ~ 1650 nm) side-polished fiber short-pass filters based on material dispersion [18]. The λ_c is thermo-optically tunable (no moving part) and the high cutoff efficiency (deep stopband and sharp filter skirt) can still be maintained while tuning to different wavelengths. The short-pass filter can be further incorporated into the ring cavity of an EDF to locally suppress the unwanted wavelengths and achieve a

high efficiency tunable fiber laser [38]. However, a single local λ_c is inefficient for the standard EDFs (no depressed inner cladding) to be operated as an amplifier at the shorter wavelengths (S-band) of the gain bandwidth. Consequently, we employ multi-stage in-line tunable fused-tapered fiber short-pass filters discretely located in the standard silica-based EDF to achieve the S-band amplification in this work. When the short-pass is turned on, the C + L-band ASE is suppressed to obtain S-band gain. On the contrary, the gain will return to the C + L-band. Hence, based on the λ_c induced by material dispersion, the EDFA can be tuned to cover the S- and C + L-bands in a simple and cost-effective way.

3.4.2 Experimental Results and Discussion

To obtain sufficient S-band amplification through standard EDFs, it is crucial to achieve tunable high-cutoff-efficiency λ_c with a high distribution density along the EDF to suppress the C + L-band ASE and maintain the high population inversion (at least 70% population inversion to obtain positive net cross section) in the S-band. The higher cutoff efficiency and a higher distribution density can make an S-band EDFA have a lower noise figure and higher gain efficiency. The cutoff efficiency of λ_c can be controlled by adjusting the material dispersion and waveguide structure of the short-pass filters. Clearly, it is advantageous to introduce their cutoff wavelengths being identical and moving simultaneously. The fused-tapering method was utilized to fabricate the four tapered fibers as shown in Fig. 3.11(a). Fig. 3.11(b) shows the schematic structure of the tunable EDFA, where the four fused-tapered single-mode fibers are discretely located within the 17.5-m-long EDF, spaced by sections of 3.5-m-long silica-based single-cladding EDF which is designed for C-band applications (EDFH0790: Prime Optical Fiber Corp.).

In material dispersion, a tunable λ_c with a high cutoff efficiency is highly related to the cross angle between the RID curves of the fiber and the dispersive materials [38]. A large cross angle can give rise to a sharp λ_c with a high rejection for the stopband wavelengths. The RID curves of the dispersive materials (Cargille index-matching liquids) and the SMF-28 (Corning) are shown in ref. [10]. Since the phonon energy of

silica fiber (~ 1100 cm^{-1}) is much higher than that of the dispersive materials, the spectral responses will be short-pass and the cutoff wavelength can be moved upward or downward depending on the applied heating temperature [18]. A larger thermo-optic coefficients |dn/dT| of the dispersive materials will lead to higher tuning efficiency for λ_c. In waveguide structure, the cutoff efficiency is influenced by the interaction length and the shape of the fused-tapered region [19]. The four fused-tapered fibers were individually fabricated using hydrogen flame with the torch size of 12 mm. The flame must be traveling back-and-forth during fabrication to guarantee a uniform waist with a long interaction length which induces more attenuation for stopband wavelengths. The total elongation length was about 30 mm and the diameter and length of the uniform waist were respectively measured around 26 μm and 18 mm under a 1000x CCD microscope. The Cargille index-matching liquid (n_D = 1.456 and $dn_D/dT = -3.74 \times 10^{-4}$/°C) was applied to surround the whole tapered region at different temperatures to generate a sharp λ_c. This is because the interaction length containing the tapered transition will not only make the RID curve of the tapered fiber raised [19], but also make whose dispersion slope steeper to produce a sharp λ_c. The spectral responses of the short-pass filters were measured using broadband superluminescent diodes spanning 1250 ~ 1650 nm and the best data is shown in Fig. 3.5. In Fig. 3.5, the best rejection efficiency at 28°C at 1530 nm can be as high as 55 dB and the 55 dB isolation bandwidth is around 80 nm (1450 ~ 1530 nm). From 1450 nm (T.L. = 1.62 dB) to 1530 nm (T.L. = 55.02 dB), the short-pass filter provides a very sharp roll-off curve with a 0.67 dB/nm slope at different temperatures. For the four filters, the maximal difference among the cutoff wavelengths was measured to be around 15.2 nm at 28.6°C. The average rejection efficiency and slope of roll-off curve were 46.4 dB and 0.53 dB/nm, respectively. The hydroxyl ions generated from flame induced loss of about 1.6 dB at 1.39 μm. These four tapered fibers were subsequently fusion-spliced with five segments of EDF shown in Fig. 3.11(b). The filters were then integrated on a glass substrate so that the temperature can be controlled by a TE-cooler.

To investigate the amplification characteristics in the S- and C + L-bands, a 980 nm pump laser with 135 mW fiber-pigtailed output power was launched into our EDF in a

forward pumping scheme through this work. The high-cutoff-efficiency short-pass filters in the 17.5-m-long EDF fiber can discretely suppress the unwanted ASE in the C + L-band and pass the S-band signal and 980 nm pump wavelengths. Subsequently, an input power of -25 dBm was respectively launched into the EDF for DFB laser signals in the S-, C-, and L-bands. The input signal spectra (P_i) and amplified output signal spectra (P_o) in S-band at 28.6°C are shown in Fig. 3.12(a) while in the C + L-band at 40°C are shown in Fig. 3.12(b), under 0.1 nm resolution bandwidth (RES) of optical spectrum analyzer (OSA). In the S-band, the signal gain at 1486.9 nm was measured 18.92 dB while in the C- and L-bands, the maximal signal gains at 1549.6 and 1589.4 nm were measured to be 37.18 dB and 15.19 dB, respectively. At 28.6°C, the S-band signal gradually grew with increasing pump power because the C + L-band ASE was discretely and substantially suppressed every 3.5-m-long EDF. At 40°C, the optical gain moved to the C + L-band and, as well as the conditions in conventional EDFAs, the S-band output signal turned out to suffer 7.1 dB loss compared with the input signal. The S-band signal still suffered 5.9 dB loss compared with the input signal when the pump power was further increased to 250 mW. This is due to the homogeneous broadening effect while erbium ions are doped in silica fiber and the emission cross sections are much higher in the C + L-band than in the S-band. Thus, even though a very high pump power is provided to achieve an excellent population inversion state, the net optical gain in the S-band is still very difficult to be squeezed from conventional EDF when the ASE in the C + L-band is not efficiently suppressed. The measured signal gains in the S- and C + L-bands are shown in table 3.3. For this proto-type tunable EDFA using discrete ASE filters, λ_c of the tapered short-pass filters can be further improved to come closer to enhance the S-band signal gain. In addition, the EDF itself can be directly tapered to serve as short-pass filters so that the splicing losses such as the splicing losses between SMF-28 fiber and EDF can be avoided. In this work, the splicing loss between SMF-28 fiber and EDF is about 0.35 dB and there are 8 splicing points to cause 2.8 dB splicing losses. The large splicing loss comes from the mismatch between the numerical aperture of the SMF-28 (NA = 0.13) and EDFH0790 (NA = 0.2).

In conclusion, we have demonstrated thermo-optically tunable EDFAs using a 17.5-m-long silica-based single-cladding C-band EDF with discrete ASE filters. The short-pass filters can provide widely tunable λ_c with a high cutoff efficiency such that the amplification of EDFA can be tuned to cover the S- and C + L-bands over 1490 ~ 1610 nm. The S-band signal gain can be further improved by using high-cutoff-efficiency short-pass filters with identical λ_c, increasing distribution density of the short-pass filters, extending the fiber length, and employing a bidirectional pumping scheme. This method can also be readily implemented in other kinds of optical amplification systems e.g., Raman amplifiers. Moreover, this tunable EDFA is very simple, cost-effective, and compatible to the conventional EDFAs in the C- and L-bands.

3.5 Diffractive-Pumped Evanescent Amplification

This section will discuss the influence of material dispersion in fiber active components. The material dispersion discrepancy between the side-polished fiber and gain medium can lead to a poor pumping efficiency of evanescent amplification. It can be improved to achieve cw-pumped evanescent gain by a diffractive-pumping method. Moreover, the importance of long interaction length between polished fiber and gain medium with highly Er^{3+} ions doping will also be discussed.

3.5.1 Diffractive-Pumping Method

The major pumping schemes for fiber amplifiers and lasers can be distinguished into core-pumping [39], cladding-pumping [40], side-pumping [41], and evanescent-pumping [42-45]. The core-pumping method was shown to have the best quantum efficiency while the cladding- and side-pumping are for high pump power delivering purposes. However, the problems of gain-robbing and noise-raising caused by the guided amplified spontaneous emission (ASE) in core are unavoidable. Though most of the ASE noise can be removed by filters, the residual noise having the same

wavelength with signals is still guided to degrade the states of polarization of the output amplified signals. This would be disadvantageous for the fiber interferometry.

In contrast, optical fibers with the passive-core and active-cladding structure were shown to have a low ASE noise based on evanescent-pumping by Sorin *et. al.* [46]. For evanescent-pumping, fiber amplifiers were successfully achieved based on side-polished fibers (SPF) [47-48]. Besides the low ASE noise, evanescent-pumping has another advantage in achieving optical amplification at any wavelength contingent on the gain medium on the SPF. This is quite difficult to realize for other above pumping schemes since many of the low phonon energy glasses are excellent host glass for e.g., Pr^{3+}, Nd^{3+}, Ho^{3+}, Tm^{3+} ions but are not suitable to be drawn into fibers because the crystallization makes the intrinsic losses highly raised [49]. By attaching the gain medium onto the SPF, the pump light excites the gain medium to give rise to stimulated emission for the incident signals via the exponential decay evanescent fields. The stimulated photons follow the direction of the reflected signals instead of the incident pump lights, thereby being subsequently guided inside the core and propagate forward [50]. The spontaneous emissions occur outside the SPF and escape away while only fractions of them satisfying the phase-matching condition can be coupled back to propagate in core and amplified, which makes the ASE naturally depressed. However, the evanescent-pumping is inefficient since the evanescent gain is highly relevant to the overlap between the local signal and pump beam intensity as well as their interaction length along the gain medium [44]. Hence, previous works [47-48] were not successful in cw-pumping. The inefficient evanescent-pumping was imputed to the short effective interaction length L_{eff} (1 ~ 2 mm) [47-48] and poor overlap among the gain medium and evanescent fields of the signal and pump lights, ascribing to dispersive evanescent wave tunneling [18] in which the index difference between the gain medium and SPF goes up when wavelength goes down. Consequently, the pump light is more tightly confined in core than the signals and its penetration of evanescent field is too weak to make the gain medium in sufficient population inversions. It is worthy noting that a heavily doped and heavily pumped gain medium is important to high gain efficiency and low noise figure.

In this work, a diffractive-pumping scheme is proposed to improve the evanescent amplification and the cw-pumped evanescent amplification is investigated based on a heavily Er^{3+}-doped fluorophosphates glass (EDFG) attached onto the SPF with long L_{eff}. A relative gain of around 2 dB at 1.55 μm wavelength is achieved and, to the best of our knowledge, this is the first time that a cw-pumped evanescent amplification using a laser glass and operating at communication wavelengths is successfully demonstrated. In our diffractive-pumping scheme, a 10° tilted fiber grating is inscribed in interaction region of the SPF to spatially separate the signal and pump lights, which can be efficiently diffracted toward the gain medium, as shown in Fig. 3.13, despite the highly dispersive evanescent wave tunneling between the SPF and gain medium.

3.5.2 Experimental Results and Discussion

For evanescent amplification, a heavily doped and heavily pumped gain medium is a key issue to achieve high gain coefficient within a short interaction length since the typical L_{eff} of the SPF is of only a few millimeters. However, the traditional Er^{3+} doped silica glass has low doping concentration, sharp and narrow gain profile around 1.55 μm, a host glass with high Er^{3+} doping ability and high quantum efficiency must be required for cw-pumped evanescent amplification. Since a low refractive index is another concern at the same time, fluorophosphate glass, which performs low n_D, high Er^{3+} concentration, high quantum efficiency, large absorption/emission cross section, wide and flat gain bandwidth shown in Fig. 3.14 is the best candidate for this work. Unfortunately, fluorophosphate glass with a high Er^{3+} concentration (> 10^{21} ions/cm^3) and a low refractive index (n_{1550} < 1.47) without concentration quenching is very difficult to achieve since such a high doping density induces high n_D value and much larger inclination to devitrify. Our EDFG was made from Shanghai Institute of Optics and Fine Mechanics, Chinese Academy of Sciences. This is the firstly reported laser glass with such low n_D, high Er^{3+} concentration and no quenching. Nevertheless, the ion pairs increase with doping concentration and can reduce the pumping efficiency and optical gain. This EDFG is highly-enriched with fluoride with its glass composition described in mol% as

$32AlF_3 11.5MgF_2 11.5CaF_2 11.5SrF_2 10.5BaF_2 3KF 9YF_3 6ErF_3 5Ba(PO_3)_2$ and the parameters of the EDFG are shown in table 3.4. The fluorescence lifetime (τ_f) was measured to be 9 ms using HP546800B100-MHz oscilloscope and its Er^{3+} concentration is much higher than that of the standard erbium-doped fibers, of the order of 10^{18}. To effectively guiding the fundamental mode, the index of the EDFG should be lower than the n_{eff} of the SPF so as to keep the active-side *V*-value in the ranging of 0.6 to 2.405 [46].

Since the refractive index of the EDFG is still much higher than the silica, a high NA fiber is necessary to meet the requirements for total internal reflection. The single-mode fiber used is HNA15A8 (Prime Optical Fiber Corp.) with NA, core and cladding diameters equal to 0.28, 3.75 μm and 80 μm, respectively. It contains 25 mol.% Ge in core and was hydrogenated to improve photosensitivity. A 10° tilted grating was inscribed with the period of 501 nm and the length of 8 mm. A longer length and a stronger index modulation of the grating are beneficial to obtain broadband diffraction for efficiently coupling the broadband 1480 nm pump laser light into radiation modes. During fabrication, a broadband 1480 nm superluminescent diode (1480-SLD) was used to measure the transmission and reflection spectra of the blazed grating as shown in Fig. 3.15(a), where the diffraction efficiency for 1479.76 nm (λ_{blaze}) is estimated to be 97.76%. Before side-polishing, the diffraction orientation of the grating was fixed and the fibers were then embedded and glued into the curved Si V-grooves for precision polishing [18]. The radius of curvature *R* of the V-grooves is 30 m and the central remained cladding thickness was 0.5 μm after polishing. The n_{eff} and the L_{eff} of the SPF at 1.55 μm wavelength were respectively calibrated to be 1.466 and 16 mm by liquid-drop experiments [18]. This L_{eff} is much longer than previous works [47-48] and that is one of the key factors to obtain a cw-pumped evanescent gain.

To investigate the dispersive evanescent wave tunneling between the EDFG and SPF, the white light sources comprising multiple SLDs of 980 nm and of from 1250 to 1650 nm wavelength were respectively launched into the side-polished HNA15A8 fiber (HNA-SPF) while the EDFG overlaying the polished surface with a low-index Cargille liquid (n_D = 1.440) at the interface. Since the refractive index of the EDFG is

higher than n_{eff} of the HNA-SPF at 1550 nm wavelength, the waveguiding was deteriorated at 1550 nm and the transmission output power became strongly lossy. However, a large amount of power was still confined to propagate in core for 980 nm wavelength and which means that the evanescent wave tunneling between the EDFG and HNA-SPF is quite dispersive [18] and thus optical amplification based on the cw evanescent-pumping turns out to be very difficult. Subsequently, the DFB signal laser lights of 1530, 1550, and 1570 nm were respectively launched into the HNA-SPF with a blazed grating inside via a 40× objective while the 250 mW 1480 nm pump laser light was simultaneously coupled into the fiber. The coupling efficiency is only about 26% for 1480 nm and 20% for 1550 nm wavelength. At this stage our exposed narrow-band blazed Bragg gratings were still too weak to greatly manifest the advantages of the diffractive-pumping. A blazed chirped grating may be employed to efficiently diffract the broadband pump light in the future. By attaching the 13.4-mm-long EDFG on the HNA-SPF to investigate the signal gain, plenty of the pump and signal powers were refracted outside the SPF since the refractive index of the EDFG is higher than n_{eff} of the SPF. For the remained reflected signal powers, the characteristics of the relative gain are shown in Fig. 3.15(b) where the pump power represents the total output power of the pump laser but not the net absorption power of the EDFG. A maximum 2 dB relative gain to be saturated at 1530 nm wavelength was successfully measured. Though only the relative gain was obtained, the net gain was promising since this heavily doped glass was heavily pumped by the refracted pump light. Since the EDFG was well pumped by the refracted pump light, the refracted signals were also amplified through the EDFG, but merely were not guided. Once a low index EDFG is available, the net gain will be achieved. The saturation gain can be improved by enhancing the optical uniformity of the EDFG to suppress the generations of phonons, which can be down by decreasing Er^{3+} concentration to (8~9) × 10^{20} ions/cm^3. In Fig. 3.15(b), the inset shows the refracted multi-step cooperative up-conversion fluorescence excited by the refracted 1480 nm pump laser and their emission spectra were 525 ~ 535 nm ($^2H_{11/2} \rightarrow {}^4I_{15/2}$ multiplet) and 535 ~ 562 nm ($^4S_{3/2} \rightarrow {}^4I_{15/2}$ multiplet).

We have demonstrated the first cw-pumped evanescent amplification at the

communication wavelengths by using a heavily Er^{3+}-doped fluorophosphates glass on the side-polished fiber. This heavily doped and heavily pumped laser glass and the 16-mm-long effective interaction length of the polished fiber make the cw-pumped evanescent amplification successful. The Er^{3+} concentration is almost thousand times higher than that of the standard erbium-doped fiber without clustering. The up-conversion fluorescence resulted from the ion pairs is interesting for the future study on up-conversion fiber lasers. Based on the diffractive-pumping method, a blazed chirped grating centered at 980 nm with wider diffraction bandwidth is expected to greatly improve the gain efficiency for ultra-low-noise Er^{3+}-doped fiber amplifiers as high sensitivity photomultipliers in the future.

References

[1] K. McCallion, W. Johnstone, and G. Fawcett, "Tunable in-line fiber-optic bandpass filter," Opt. Lett. **19,** 542-544 (1994).

[2] S. G. Lee, J. P. Sokoloff, B. P. McGinnis, and H. Sasabe, "Fabrication of a side-polished fiber polarizer with a birefringent polymer overlay," Opt. Lett. **22,** 606-608 (1997).

[3] W. V. Sorin and M. H. Yu, "Single-mode-fiber ring dye laser," Opt. Lett. **10,** 550-552 (1985).

[4] F. Pan, K. McCallion, and M. Chiappetta, "Waveguide fabrication and high-speed in-line intensity modulation in 4-N, N-48-dimethylamino-48-N8-methyl-stilbazolium tosylate," Appl. Phys. Lett. **74**, 492-494 (1999).

[5] S. S. Johal, S. W. James, R. P. Tatam, and G. J. Ashwell, "Second-harmonic generation in Langmuir-Blodgett waveguide overlays on single-mode optical fiber," Opt. Lett. **24,** 1194-1196 (1999).

[6] D. Flannery, S. W. James, R. P. Tatam, and G. J. Ashwell, "pH sensor using Langmuir-Blodgett overlays on polished optical fibers," Opt. Lett. **22,** 567-569 (1997).

[7] G. Raizada and B. P. Pal, "Refract meters and tunable components based on side-polished fibers with multimode overlay waveguides: role of the supersaturate," Opt. Lett. **21,** 399-401 (1996).

[8] J. W. Yu and K. Oh, "New in-line fiber band pass filters using high silica dispersive optical fibres," Opt. Commun. **204,** 111-118 (2002).

[9] K. Morishita, "Optical fiber devices using dispersive materials," J. Lightwave Technol. **7,** 198-201 (1989).

[10] K. Morishita, "Bandpass and band-rejection filters using dispersive fibers," J. Lightwave Technol. **7,** 816-819 (1989).

[11] J. Nishimura and K. Morishita, "Mode-field expansion and reduction in dispersive fibers by local heat treatments," J. Select. Topics Quantum Electron. **5,** 1260-1265 (1999).

[12] M. Tammer, R. W. T. Higgins, and A. P. Monkman, "High optical anisotropy in thin film of polyfluorene and its affect on the outcoupling of light in typical polymer light emitting diode structures," J. Appl. Phys. **91,** 4010-4013 (2002).

[13] H. R. Stuart, "Dispersive multiplexing in multimode optical fiber," Science **289,** 281-283 (2000).

[14] N. K. Chen, S. Chi, and S. M. Tseng, "Narrow-band channel-dropping filter based on side-polished fiber with long interaction length," Jpn. J. Appl. Phys. **43,** L475-L477 (2004).

[15] O. Leminger and R. Zengerle, "Determination of the variable core-to-surface spacing of single-mode fiber-coupler blocks," Opt. Lett. **12,** 211-213 (1987).

[16] A. K. Das, M. A. Mondal, A. Mukherjee, and A. K. Mandal, "Automatic determination of the remaining cladding thickness of a single-mode fiber half-coupler," Opt. Lett. **19,** 384-386 (1994).

[17] N. K. Chen, K. C. Hsu, H. J. Chang, S. Chi, and Y. Lai, "Tunable Er^{3+}/Yb^{3+} codoped fiber amplifiers covering *S*- and *C*-Bands (1460 ~ 1580 nm) based on discrete fundamental-mode cutoff," in *Proceedings of* ***OFC 2006*** conference, Anaheim, USA, Mar. 5-10, 2006. OThJ5.

[18] N. K. Chen, S. Chi, and S. M. Tseng, "Wideband tunable fiber short-pass filter based on side-polished fiber with dispersive polymer overlay," Opt. Lett. **29**, 2219-2221 (2004).

[19] J. Villatoro, D. Monzon-Hernandez, and D. Luna-Moreno, "In-line tunable band-edge filter based on a single-mode tapered fiber coated with a dispersive material," IEEE Photon. Technol. Lett. **17**, 1665-1667 (2005).

[20] N. K. Chen and S. Chi, "Spectral characteristics of side-polished endlessly single-mode photonic crystal fiber: waveguide dispersion," in proceedings of ***OFC 2006*** conference, Anaheim, USA, Mar. 5-10, 2006. OWI5

[21] D. A. Smith, M. W. Maeda, J. J. Johnson, J. S. Patel, M. A. Saifi, and A. Von Lehman, "Acoustically tuned erbium-doped fiber ring laser," Opt. Lett. **16**, 387-389 (1991).

[22] Y. W. Song, S. A. Havstad, D. Starodubov, Y. Xie A. E. Willner, and J. Feinberg, "40-nm-wide tunable fiber ring laser with single-mode operation using a highly stretchable FBG," IEEE Photonics Technol. Lett. **13**, 1167-1169 (2001).

[23] B. O. Guan, H. Y. Tam, H. L. W. Chan, X. Y. Dong, C. L. Loong, and M. S. Demokan, "Temperature-tuned erbium-doped fiber ring laser with polymer-coated fiber grating," Opt. Commun. **202**, 331-334 (2002).

[24] S. Yamashita and M. Nishihara, "Widely tunable erbium-doped fiber ring laser covering both C-band and L-band," IEEE J. Sel. Top. Quantum Electron. **7**, 41-43 (2001).

[25] K. R. Sohn and J. W. Song, "Thermooptically tunable side-polished fiber comb filter and its application," IEEE Photonics Technol. Lett. **14**, 1575-1577 (2002).

[26] K. R. Sohn and K. Taek, "Multiwavelength all-fiber ring laser using side-polished fiber comb filter and mechanically formed long-period fiber gratings," IEEE Photonics Technol. Lett. **17**, 309-311 (2005).

[27] A. Gloag, N. Langford, K. McCallion, and W. Johnstone, "Tunable, single frequency erbium fiber laser using an overlay bandpass filter," Appl. Phys. Lett. **66**, 3263-3265 (1995).

[28] A. Gloag, N. Langford, K. McCallion, and W. Johnstone, "Tunable erbium fiber laser using an overlay bandpass filter," Opt. Lett. **19**, 801-803 (1994).

[29] M. A. Arbore, "Application of fundamental-mode cutoff for novel amplifiers and lasers," in *Proceedings of Optical Fiber Communication Conference OFC'05 (Optical Society of America, Washi*ngton, D.C., 2005), paper OFB4.

[30] M. A. Arbore, Y. Zhou, H. Thiele, J. Bromage, and L. Nelson, "S-band erbium-doped fiber amplifiers for WDM transmission between 1488 and 1508 nm," in *Proceedings of Optical Fiber Communication Conference OFC'03 (Optical Society of America, Washington, D.C., 2003)*, paper WK2.

[31] M. Monerie, "Propagation in doubly clad single-mode fibers," IEEE J. Quantum Electron. **QE-18**, 535-542 (1982).

[32] S Shen, A. Jha, L. Huang, and P. Joshi, "980-nm diode-pumped Tm^{3+}/Yb^{3+}-codoped tellurite fiber for *S*-band amplification," Opt. Lett. **30,** 1437-1439 (2005).

[33] S. S. H. Yam, M. E. Marhic, Y. Akasaka, and L. G. Kazovsky, "Gain-clamped *S*-band discrete Raman amplifier," Opt. Lett. **29,** 757-759 (2004).

[34] H. S. Seo, W. J. Chung, and J. T. Ahn, "*S* + *C* bands amplification in a distributed Er-doped Raman fiber," IEEE Photonics Technol. Lett. **17**, 1181-1183 (2005).

[35] H. Ono, M. Yamada, and M. Shimizu, "*S*-band erbium-doped fiber amplifiers with a multistage configuration–design, characterization, and gain tilt compensation," J. Lightwave Technol. **21**, 2240-2246 (2003).

[36] J. B. Rosolem, A. A. Juriollo, R. Arradi, A. D. Coral, J. C. R. F. Oliveira, and M. A. Romero, "All silica *S*-band double-pass erbium-doped fiber amplifier," IEEE Photonics Technol. Lett. **17**, 1399-1401 (2005).

[37] K. Thyagarajan and C. Kakkar, "*S*-band single-stage EDFA with 25-dB gain using distributed ASE suppression," IEEE Photonics Technol. Lett. **16**, 2448-2450 (2004).

[38] N. K. Chen, S. Chi, and S. M. Tseng, "An efficient local fundamental-mode cutoff for thermo-optic tunable Er^{3+}-doped fiber ring laser," Opt. Express **13**, 7250-7255 (2005).

[39] M. Nakazawa, Y. Kimura, and K. Suzuki, "Efficient Er^{3+}-doped optical fiber amplifier pumped by a 1.48 μm InGaAsP laser diode," Appl. Phys. Lett. **54**, 295-297 (1989).

[40] R. Selvas, J. K. Sahu, L. B. Fu, J. N. Jang, J. Nilsson, A. B. Grudinin, K. H. Ylä-Jarkko, S. A. Alam, P. W. Turner, and J. Moore, "High-power, low-noise, Yb-doped, cladding-pumped, three-level fiber sources at 980 nm," Opt. Lett. **28**, 1093-1095 (2003).

[41] L. Goldberg, J. P. Koplow, and D. A. V. Kliner, "Highly efficient 4-W Yb-doped fiber amplifier pumped by a broad-strip laser diode," Opt. Lett. **24**, 673-675 (1999).

[42] H. J. Moon, Y. T. Chough, and K. An, "Cylindrical microcavity laser based on the evanescent-wave-coupled gain," Phys. Rev. Lett. **85**, 3161-3164 (2000).

[43] T. Ohtsuki, S. Honkanen, N. Peyghambarian, M. Takahashi, Y. Kawamoto, J. Ingenhoff, A. Tervonen, and K. Kadono, "Evanescent-field amplification in Nd^{3+}-doped fluoride planar waveguide," Appl. Phys. Lett. **69**, 2012-2014 (1996).

[44] K. O. Hill, R. I. MacDonald, and A. Watanabe, "Evanescent-wave amplification in asymmetric-slab waveguides," JOSA **64**, 263-273 (1974).

[45] N. Periasamy and F. P. Schäfer, "Laser amplification in an optical fiber by evanescent field coupling," Appl. Phys. **24**, 201-203 (1981).

[46] A. V. Astakhov, M. M. Butusov, and S. L. Galkin, "Characteristics of laser effects in active fiber lightguides," Opt. Spectrosc. (USSR) **59**, 551-553 (1985).

[47] W. V. Sorin, K. P. Jackson, and H. J. Shaw, "Evanescent amplification in a single-mode optical fibre," Electron. Lett. **19**, 820-821 (1983).

[48] V. A. Kozlov, V. V. Ter-Mikirtychev, and T. Tsuboi, "In-line singlemode fibre amplifiers based on $LiF:F_2^+$ and $LiF:F_2^-$ crystals," Electron. Lett. **31**, 2104-2105 (1995).

[49] S. Sudo, "Optical Fiber Amplifiers: Materials, Devices, and Applications," (Artech House, Boston, 1997), Ch. 1-2.

[50] C. W. Lee, K. Kim, J. Noh, and W. Jhe, "Quantum theory of amplified total internal reflection due to evanescent-mode coupling," Phys. Rev. A. **62**, Art. No. 053805 (2000).

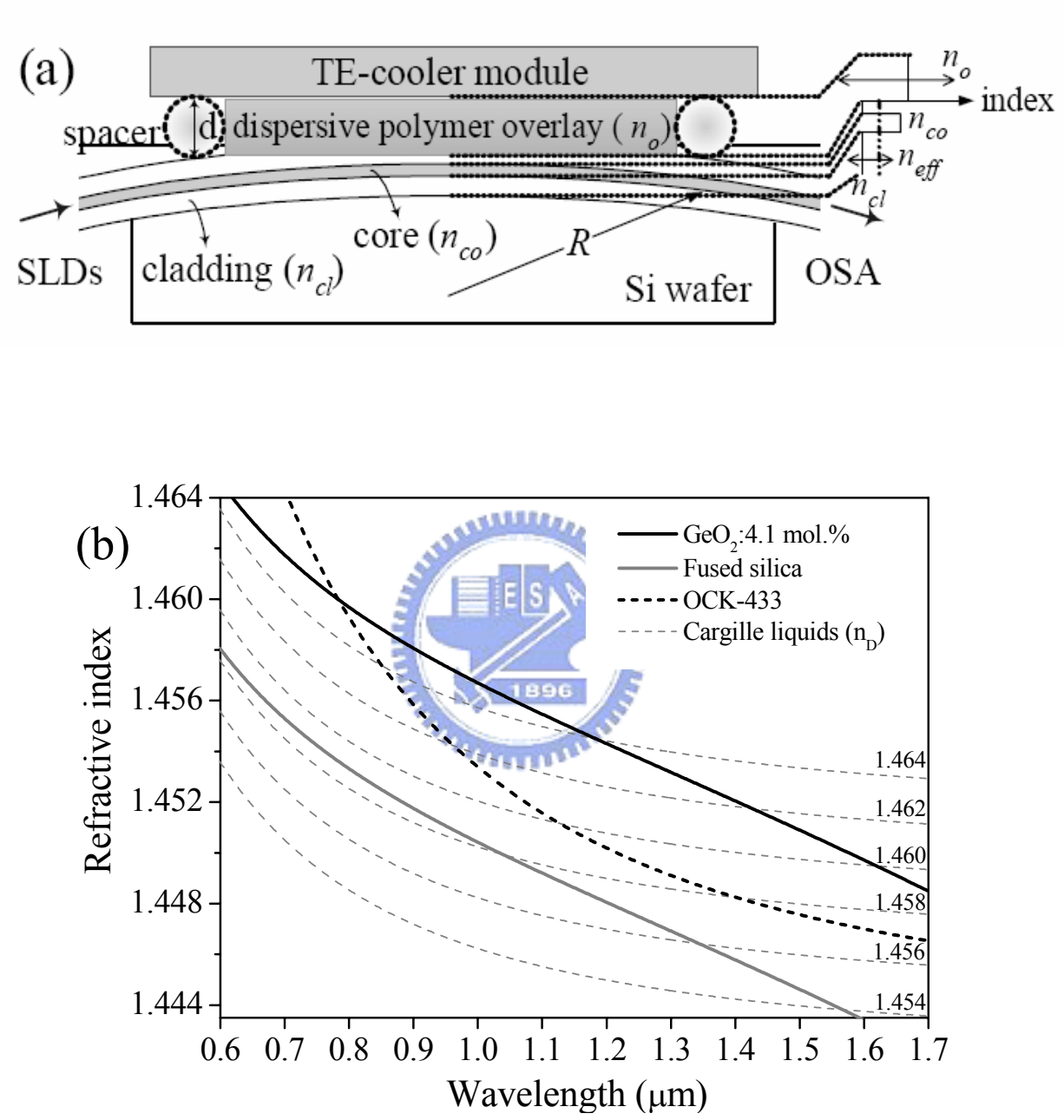

Fig. 3.1 (a) Schematic of the device. The index profile of the filter is shown at right-hand side. (b) Refractive index dispersion curves. OCK-433 is the dispersive polymer.

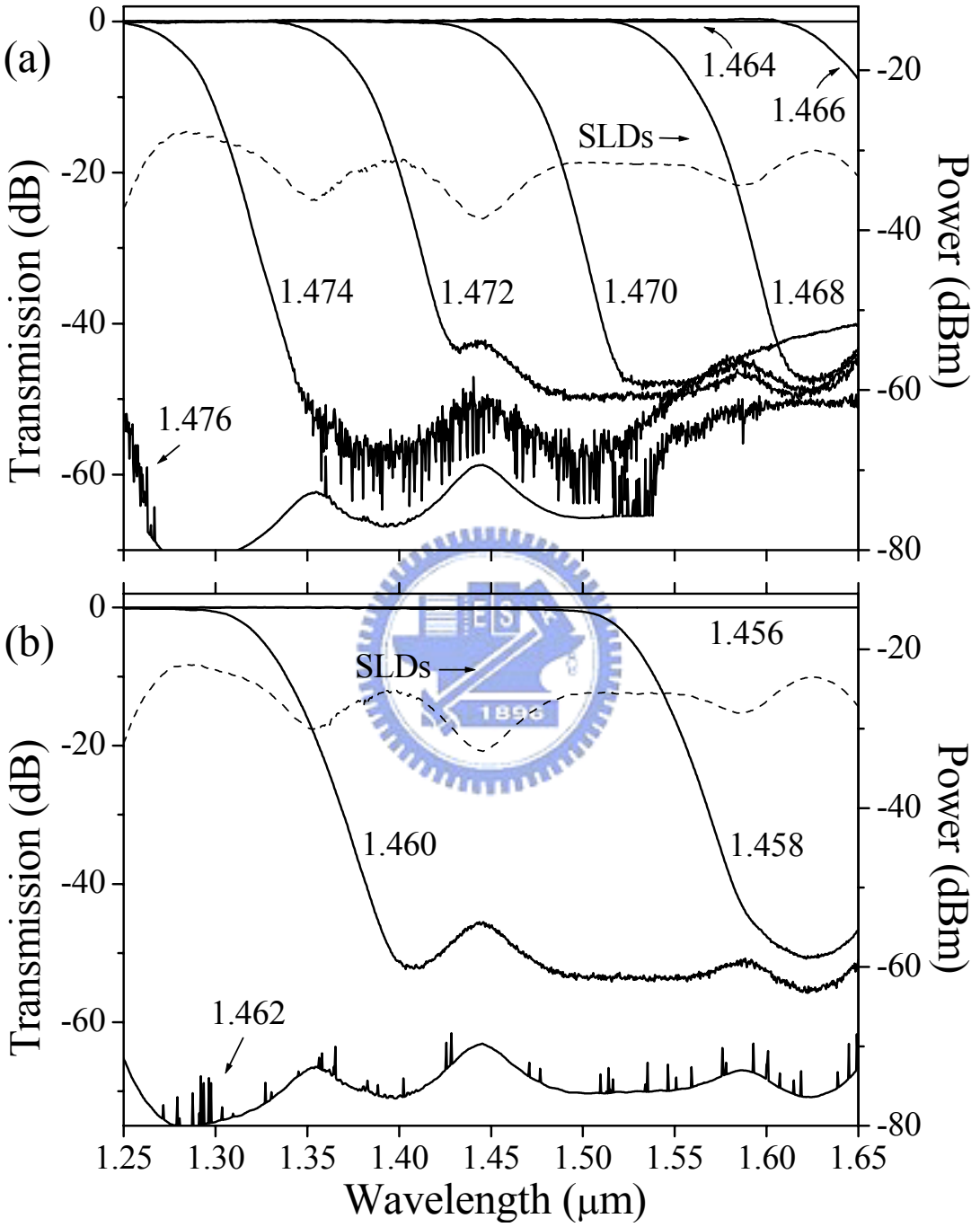

Fig. 3.2 Spectral responses of the (a) SP-GF4A (b) SP-SMF-28 with various Cargille index liquids overlay. Resolution: 1 nm. *R*: 15 m.

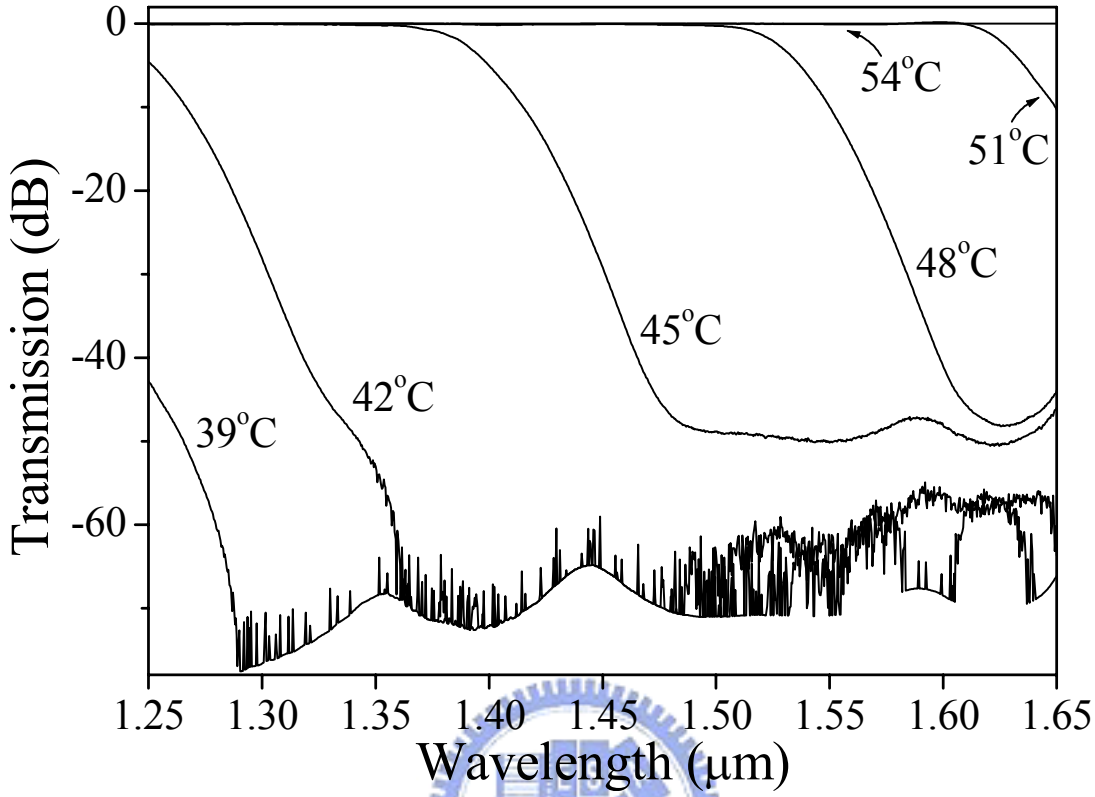

Fig. 3.3 Wavelength tunability of the short-pass filter using SP-SMF-28 with OCK-433 overlay through thermo-tuning. Resolution: 1 nm. *R*: 15 m.

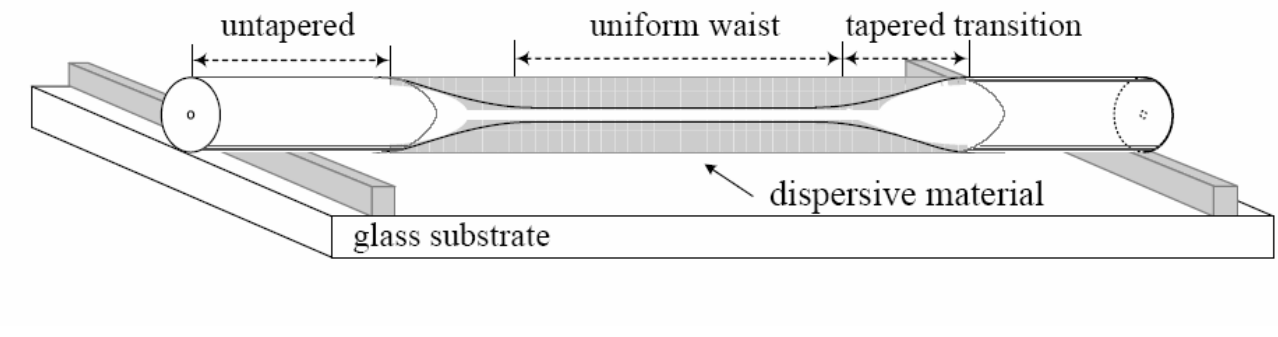

Fig. 3.4 Fused-tapered fiber short-pass filter.

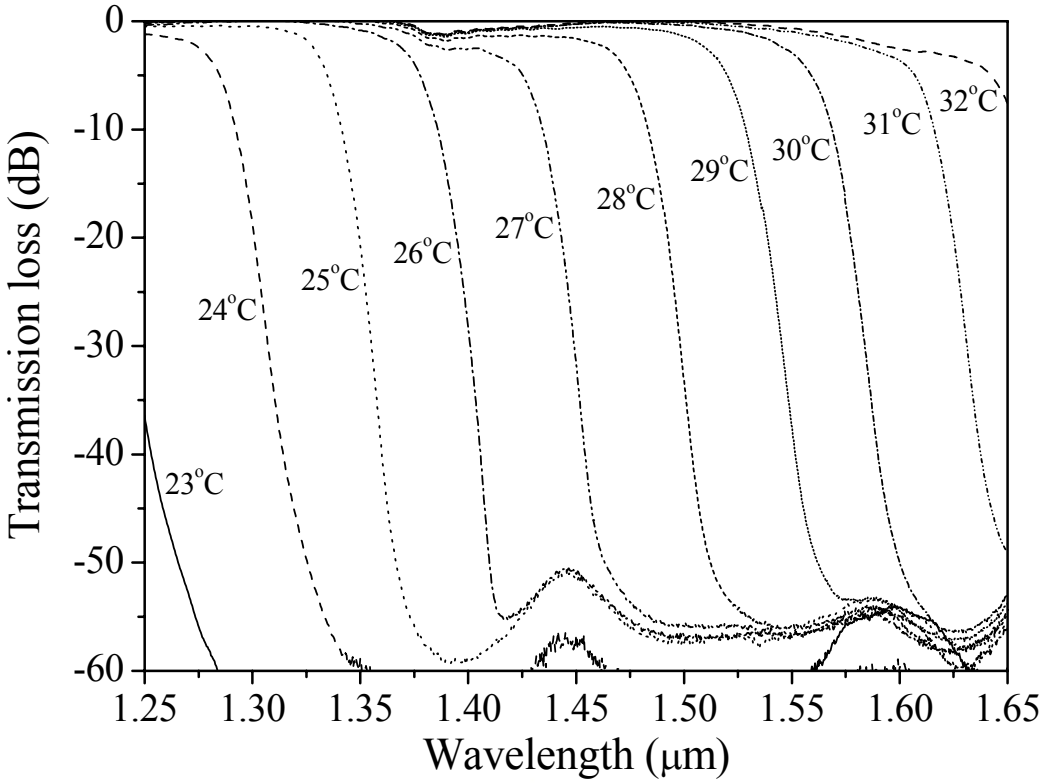

Fig. 3.5 Spectral responses of the tapered fiber short-pass filters using a Cargille liquid with n_D = 1.456 at different temperatures. (RES: 1 nm)

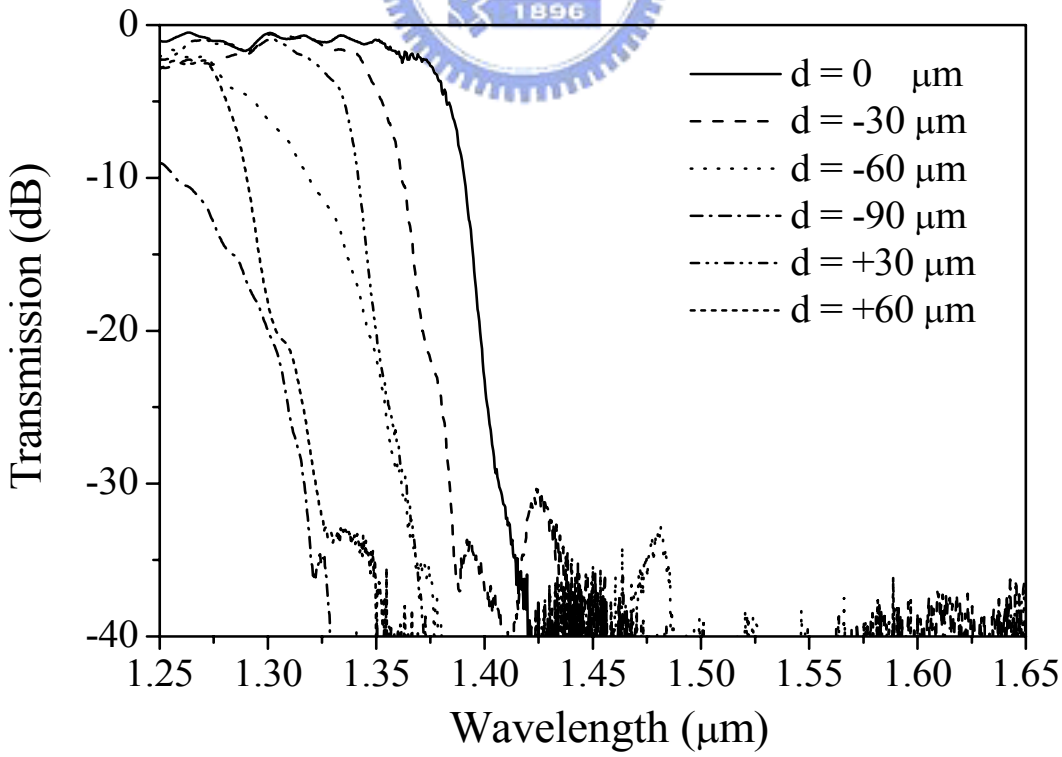

Fig. 3.6 Spectral responses of the tapered fiber in the straight and bending conditions.

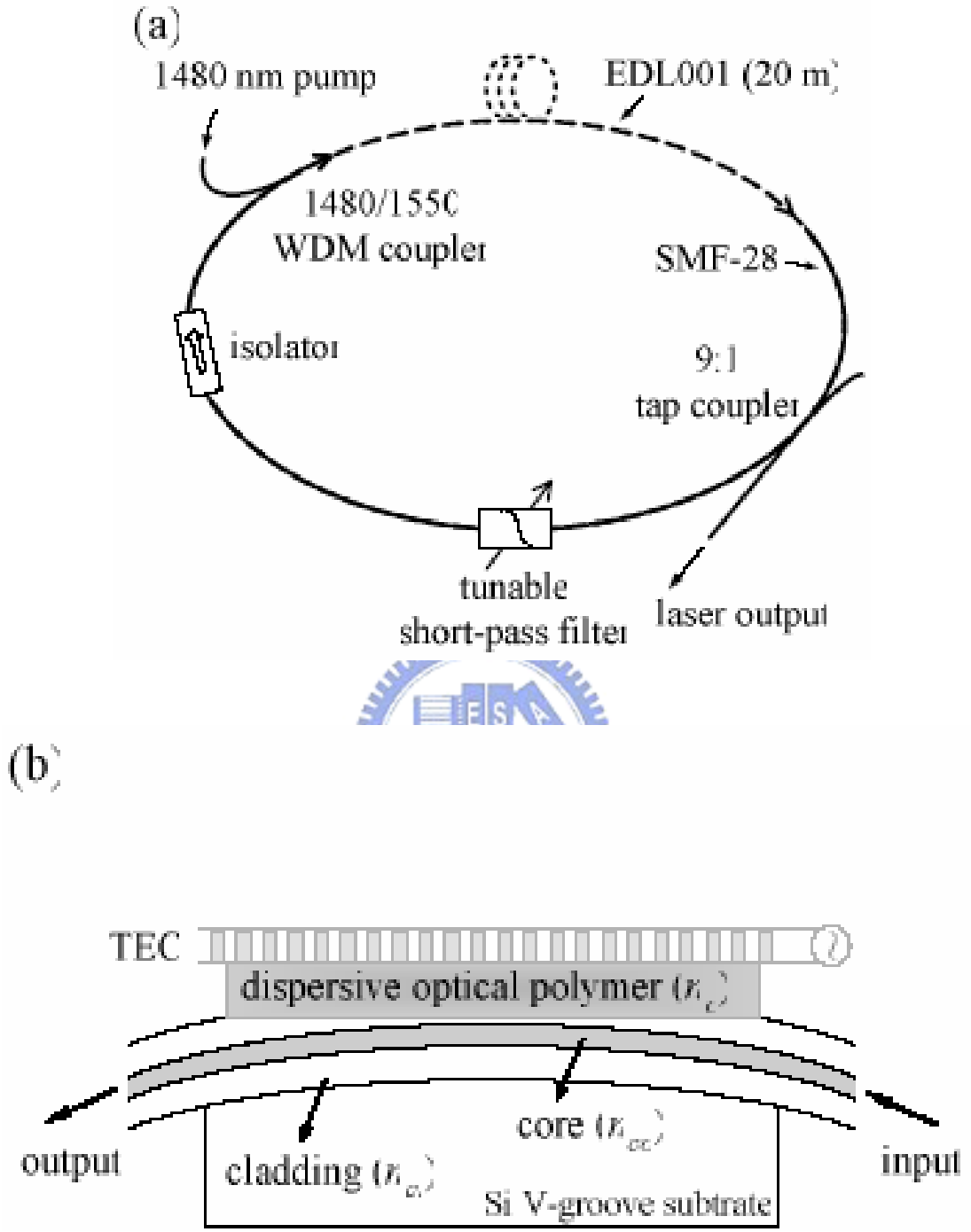

Fig. 3.7 (a) Experimental set up of the EDFRL and (b) Device structure of the side-polished fiber based tunable short-pass filter.

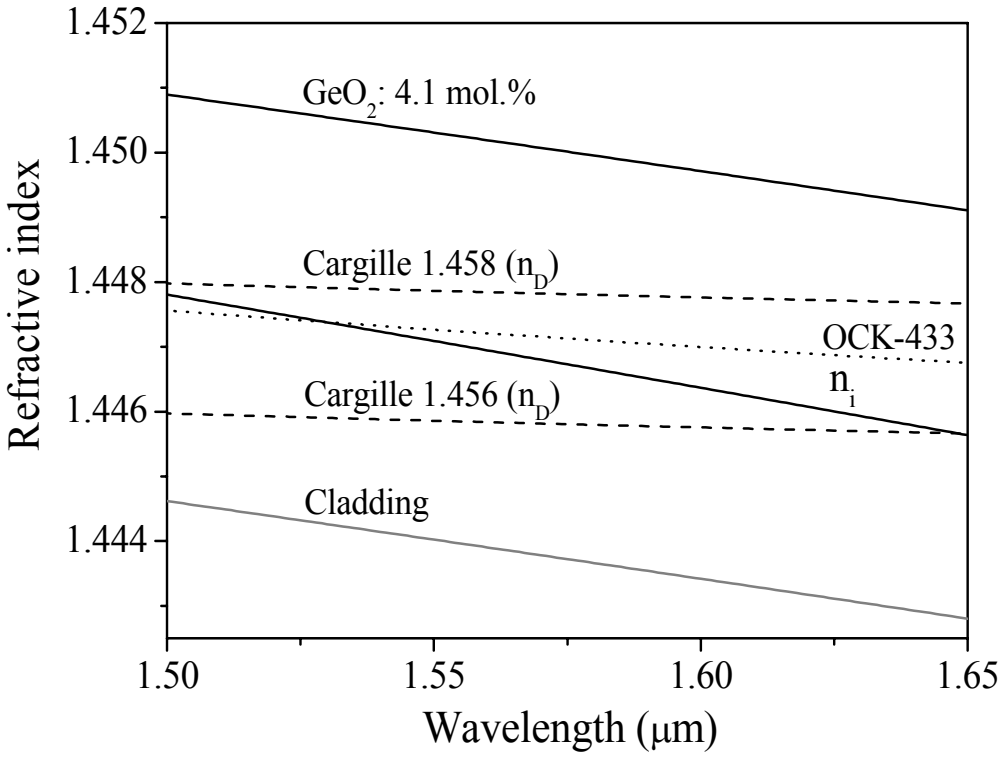

Fig. 3.8 Refractive index dispersions of the fiber, Cargille index liquids and thermo-optic polymer OCK-433.

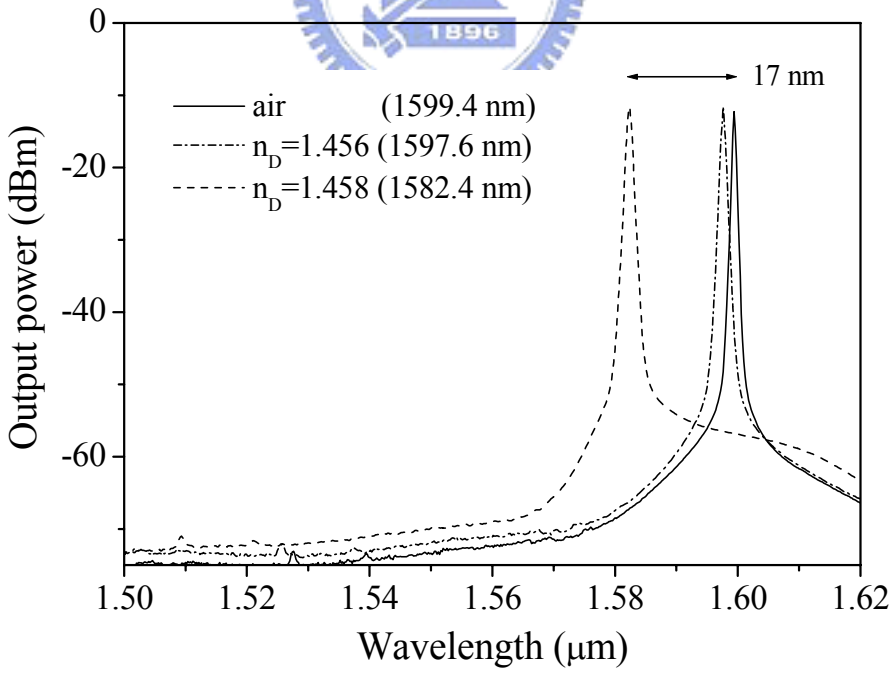

Fig. 3.9 Spectral responses of the EDFRL in air and using two Cargille index liquids on SPF.

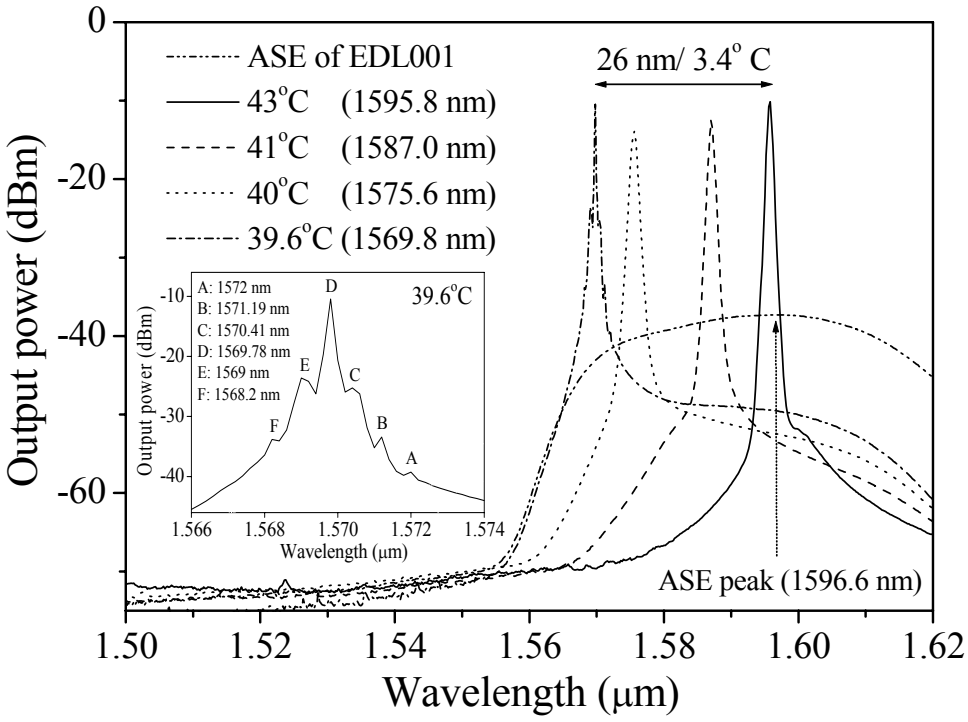

Fig. 3.10 Spectral responses of the wavelength tuning of the EDFRL when OCK-433 polymer was cooling down.

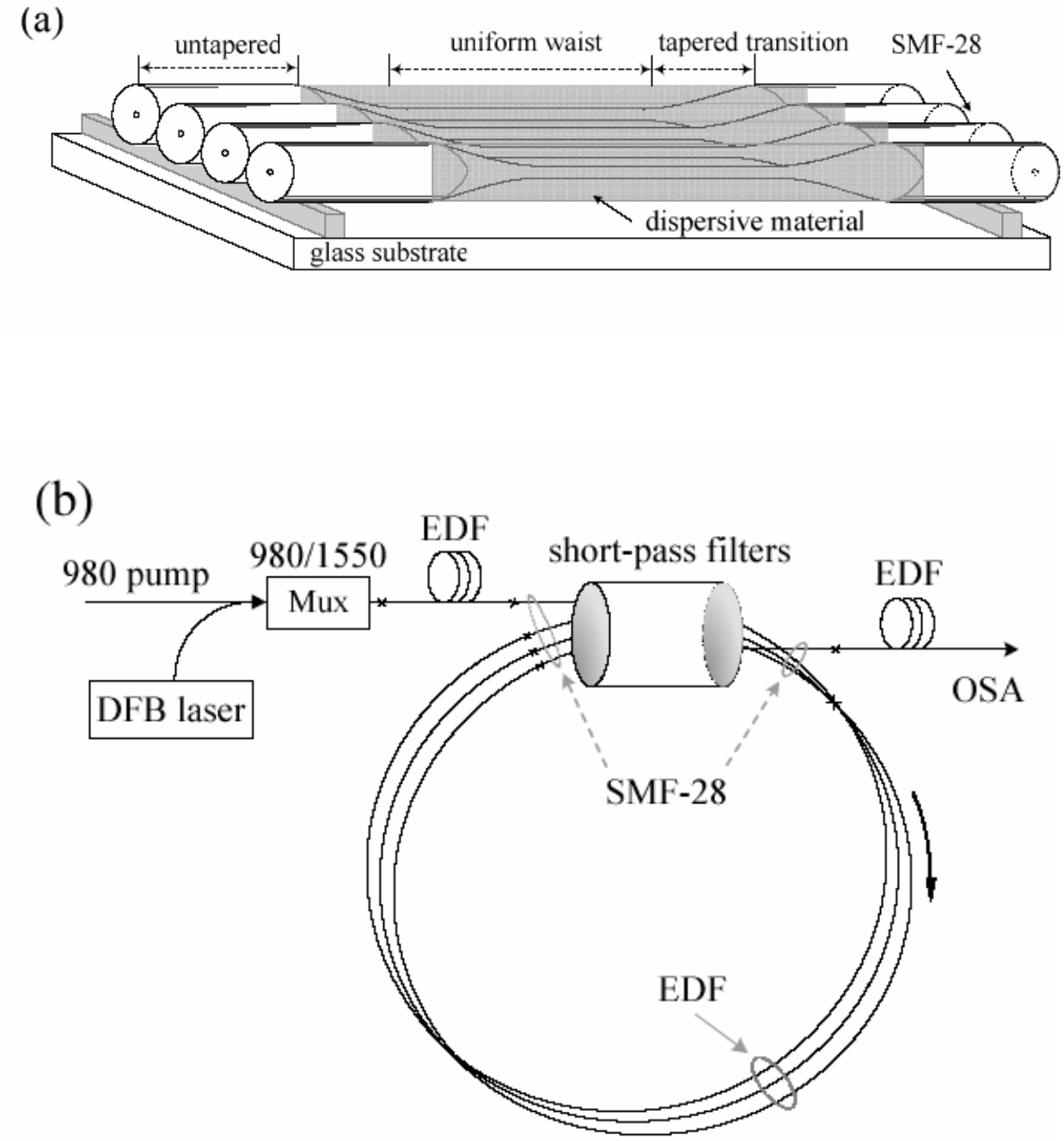

Fig. 3.11 (a) Integrated fused-tapered fiber short-pass filters with the whole tapered regions surrounded with a dispersive material. (b) Schematic of the tunable EDFA covering *S*- and *C* + *L*-bands with 17.5-m-long EDF.

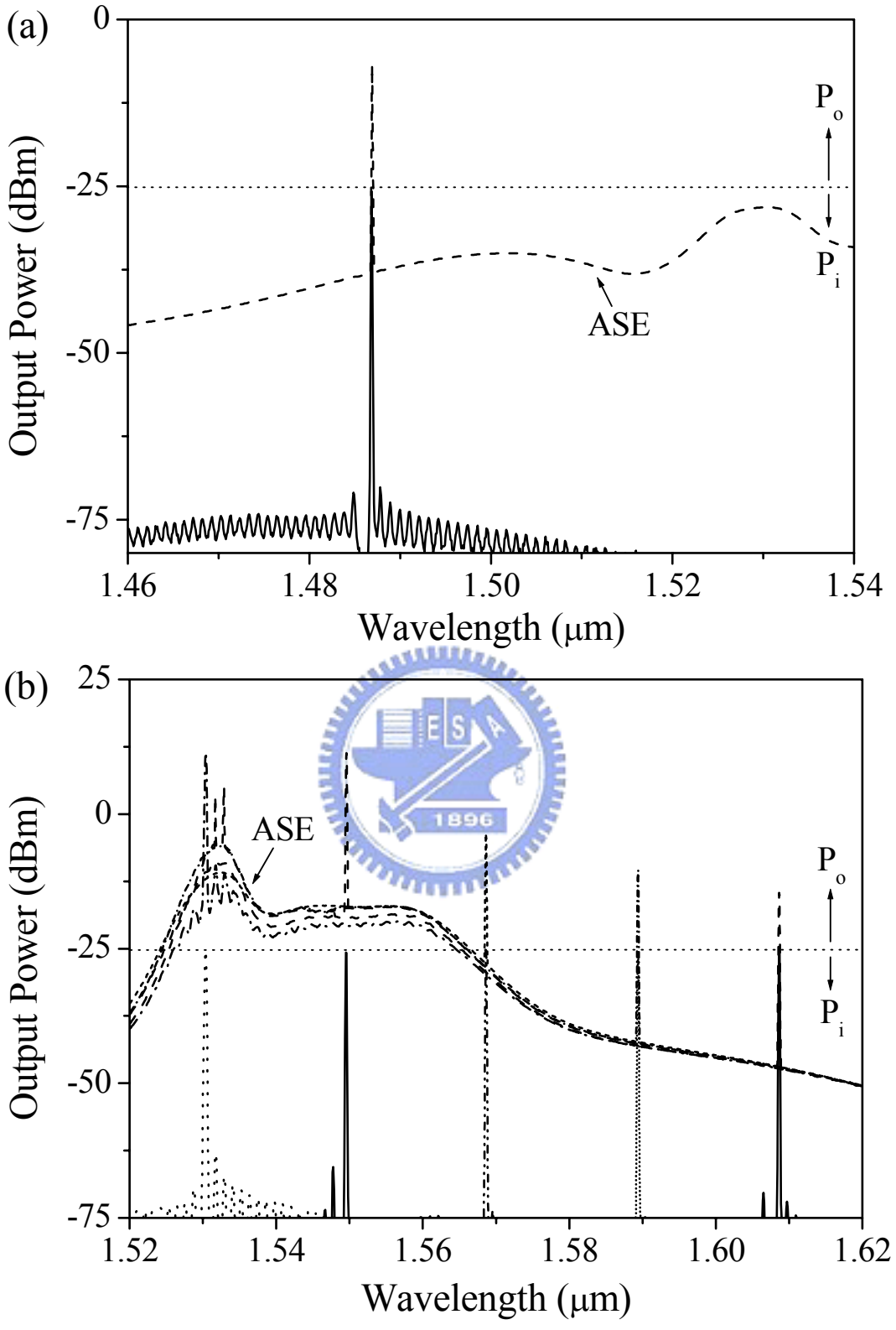

Fig. 3.12 Amplification spectra of the signals in (a) *S*-band at 28.6°C and (b) *C* + *L*-band at 40°C (RES: 0.1 nm). P_i and P_o are input and output signal spectra, respectively.

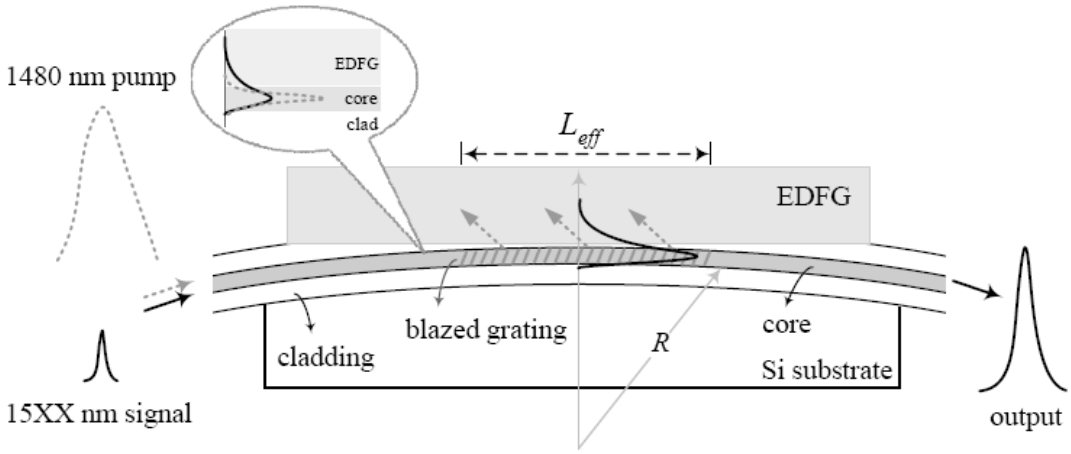

Fig. 3.13 Schematic of the proposed diffractive-pumping method. The inset shows the conventional evanescent-pumping method where the dispersive evanescent wave tunneling makes the excitation inefficient.

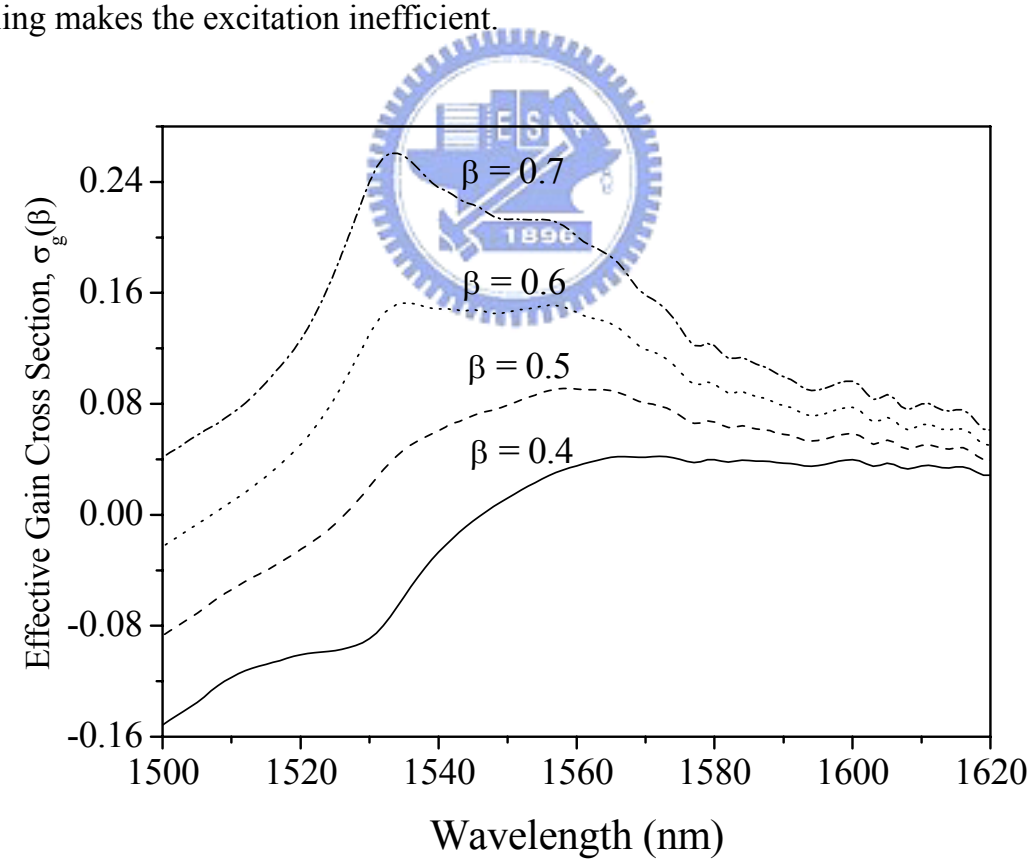

Fig. 3.14 Effective gain profile of Er^{3+} in fluorophosphate glass, β is the minimum population in the upper level. The gain coefficient change with wavelength at different pumping energies.

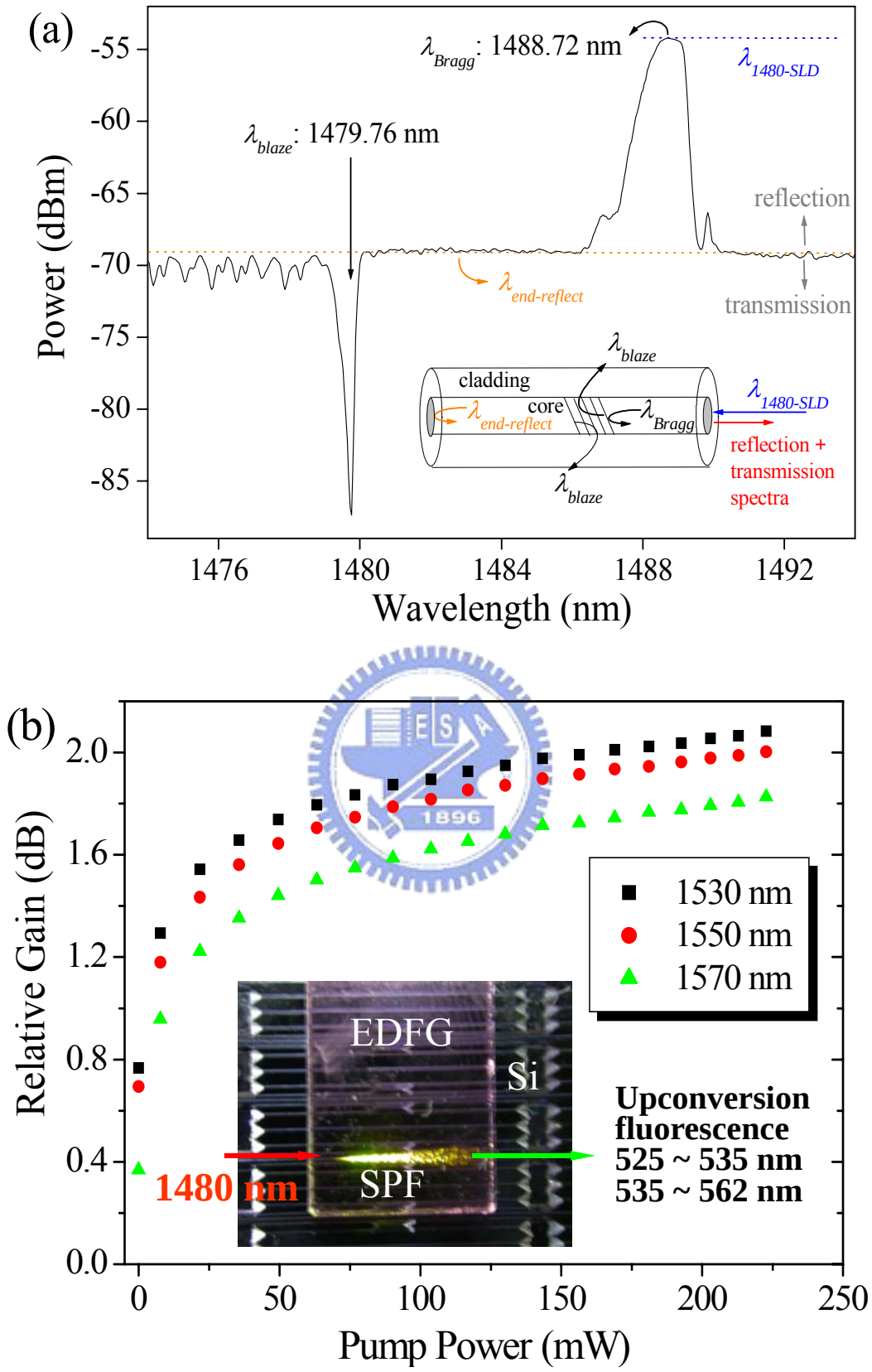

Fig. 3.15 (a) The measured transmission and reflection spectra of the blazed grating and (b) amplification characteristics of the wavelengths at 1530, 1550, and 1570 nm wavelengths.

Table 3.1 Fiber Parameters at 1550 nm wavelength

Fiber	MFD (μm)	NA	LP_{11}-λ_c (nm)	Core Diameter (μm)	Clad. Diameter (μm)
SMF-28	10.4	0.13	1260	8.2	125
GF4A	4.0	0.3	1385	3.5	35 (inner) 125 (outer)

Table 3.2 Laser linewidth of the EDFRL

Cargille liquids				
Peak wavelength (nm)	1582.4	1597.6	1599.4	
FWHM (nm)	0.75	0.47	0.42	
30 dB (nm)	3.98	3.3	2.66	
OCK-433				
Peak wavelength (nm)	1569.8	1575.6	1587.0	1595.8
FWHM (nm)	0.12	0.8	0.6	0.52
30 dB (nm)	4.84	5.15	4.22	3.4

Table 3.3 Measured signal gains in *S*- and *C* + *L*-bands.

Laser wavelength (nm)	Gain (dB)
1486.9	18.92
1530.4	36.80
1549.6	37.18
1568.6	28.89
1589.4	15.19
1608.6	10.60

Table 3.4 Parameters of the EDFG.

Dimensions (mm)	3.4 (L) × 9.8 (W) × 1.6 (H)
Density (g/cm^3)	4.02
Refractive index at 589.3 nm, n_D	1.4763
Refractive index at 1550 nm, n_{1550}	1.4695
Er^{3+} concentration, NEr^{3+} (ions/cm^3)	1.19×10^{21}
ErF_3 concentration (wt%)	11.1
Fluorescence lifetime, τ_f (ms)	9.0
Peak absorption cross section at 1530nm (cm^2)	5.43×10^{-21}
Peak emission cross section at 1532 nm (cm^2)	5.99×10^{-21}
Fluorescence linewidth, FWHM (nm)	54